Electronic Supporting Information (ESI)

Supported Ruthenium Catalyst for Transformation of Aqueous Glycerol to Hydrogen Gas and Lactic Acid

Ankit Kumar,[a] Bhanu Priya,[a] Rohit Kumar Rai,[b] Parveen Garg,[c] Uday Deshpande,[c] and Sanjay Kumar Singh*[a]

[a]Catalysis Group, Department of Chemistry, Indian Institute of Technology Indore, Simrol, Khandwa Road, Indore 453552, M. P., India.

[b]KAUST Catalysis Center and Division of Physical Sciences and Engineering, King Abdullah University of Science and Technology (KAUST), Thuwal 23955-6900, Kingdom of Saudi Arabia.

[c]UGC-DAE Consortium for Scientific Research, Indore 452001, M.P., India.

Email: sksingh@iiti.ac.in (SKS)

Calculation of TON and TOF

Turnover number (TON) and Turnover frequency were calculated using the formula given below. The gas was collected at room temperature for all the reactions.

$$TON = n(H_2)/n(catalyst)$$

$$TOF = TON/time$$

Where $n(H_2)$ is the number of millimoles of gas released, was calculated by considering $V_{m,H2,25°C}$ values from Vander Waals equation as shown in the previous work,[S1] and n(catalyst) is the millimole of catalyst used for the catalytic reaction.

Calculation of conversion, selectivity, yield, and carbon balance[S2]

$$Conversion = [C_i(GLY) - C_f(GLY)]/C_i(GLY)\times 100\ (\%)$$

$$Selectivity = C_f(P)/C_c(GLY)\times 100\ (\%)$$

$$Yield = C_f(P)/C_i(GLY)\times 100\ (\%)$$

$$Carbon\ Balance = [1\text{-}Conv._{GLY} + Y_{SL} + Y_{SG} + Y_{PD} + Y_{SF}] \times 100\ (\%)$$

Where $C_i(GLY)$ = millimoles of carbon in the initial glycerol

$C_f(GLY)$ = millimoles of carbon in the final glycerol

$C_c(GLY)$ = millimoles of carbon in the converted glycerol

$C_f(P)$ = millimoles of carbons in the final product

Calculation of metal dispersion[S3, S4]

'Metal Dispersion' describes the distribution of metal nanoparticles over the support, where high dispersion indicates that the nanoparticles are uniformly distributed, resulting in a greater surface area of the active component being available for catalysis, whereas low dispersion signifies that the nanoparticles are clustered or aggregated, thereby reducing the available active surface area. In our study, 'dispersion' refers to the particle size of Ru nanoparticles. Particle size measured using TEM is used to estimate the dispersion by assuming metal nanoparticles as spherical particles, as explained in the following sections.

- Let's consider a collection of n_i spherical particles of diameter d_i, of area A_i (or πd_i^2) and of volume V_i (or $\pi d_i^3/6$). As two mean particle sizes are usually considered, the length-number mean diameter, $d_{LN} = \Sigma n_i d_i/\Sigma n_i$ and the volume-area mean diameter, $d_{VA} = \Sigma n_i d_i^3/\Sigma n_i d_i^2$.
- The surface area occupied by an atom m on a polycrystalline surface is given by

$$a_m = 1/n_s$$

where n_s is the mean number of atoms (For Ru, a_m = 6.35 Å^2).

- The volume V_m occupied by an atom m in the bulk of the metal is given by

$$V_m = M_{Ru}/(\rho \times N_A) \quad (1)$$

where M_{Ru} = Atomic weight of Ru metal and ρ = Density of Ru metal, N_A = Avogadro's number

- The relation between specific surface area (S_{sp}) and mean particle size (d_{VA}) is

$$S_{sp} = \Sigma n_i A_i/(\rho \Sigma n_i V_i) \quad (2)$$

Since, $Ai = \pi d_i^2$ and $Vi = \pi d_i^3/6$,

$$\text{Therefore, } S_{sp} = 6/(\rho \times d_{VA}) \quad (3)$$

- The relation between specific surface area (S_{sp}) and metal dispersion (D) is

$$S_{sp} = a_m \times (N_A/M_{Ru}) \times D \quad (4)$$

- The relation between metal dispersion (D) and mean particle size (d_{VA}):
  We can write from eq. (3)

$$d_{VA} = 6/(\rho \times S_{sp}) \quad (5)$$

Using eq. (1), (4) and (5); we can write

$$d_{VA} = 6/[(a_m/V_m) \times D]$$

$$D = 6[(V_m/a_m)/d_{VA}] \quad (6)$$

Putting the value of V_m from eq. (1) in eq. (6);

$$D = (6 \times M_{Ru})/(\rho \times d_{VA} \times a_m \times N_A)$$

$$D\ (\%) = (600 \times M_{Ru})/(\rho \times d_{VA} \times a_m \times N_A) \quad (7)$$

where M_{Ru} = Atomic weight of Ru metal and ρ = Density of Ru metal

d_{VA} = Particle size in nm, estimated from TEM analysis

a_m = Atomic surface area of Ru metal

The surface area occupied by an atom (a_m) is related to the mean number of surface atoms per unit area (n_s) by the equation $a_m = 1/n_s$. For Ru, which adopts a hexagonal close-packed (hcp) structure, the number of surface atoms (n_s) was determined based on the (001) plane using the lattice parameters of ruthenium.[S4] The calculated value of a_m for Ru (6.35 Å^2) was also adopted by other authors.[S3]

Table S1 Comparison with hydrogen production systems from glycerol in the literature.

Catalyst	Solvent	Base (equiv.)	T(°C) /t(h)	Gas/ p(bar)	Conv. (%)	Sel. of LA (%)	Contaminants	Sel. of H_2/{$n(H_2)$/ n(GLY)}	Ref.
$Ru/La(OH)_3$	**water**	**NaOH (2.0)**	**130/4.5**	**Ar**	**>99**	**86**	**n. d.**	**>99.9%/1.4**	**This work**
Ru	water	NaOH (2.0)	110/10	Ar	>99	70	n. d.	>99%/1.6	S2
Ru-NMC-3	water	-	250/12	N_2/40	92	-	CO, CO_2, CH_4	88.5/-	
Ru-Pt-NMC-3	water	-	250/12	N_2/40	87.9	-	CO, CO_2, CH_4	82.2/-	S3
Ru/NaY	-	-	250/12	N_2/40	88.1	-	CO, CO_2, CH_4	68.1/-	S5
PtMo/C	water	-	230/720	Ar/31	26	-	CO_2, CH_4	55.3/-	S6
PtRe/C	water	KOH	225/-	N_2/29	58.5	-	CO, CO_2, Alkane	24.5/-	S7
Ni/Al_2O_3-La_2O_3	water	-	225/2.5	-/30	37	-	CO, CO_2, CH_4	32/-	S8
Pt-Cu/Mg(Al)O	water	-	200/5	-/29	98	-	CO, CO_2, CH_4	55.3/-	S9
Pt/Al_2O_3	water	-	225/24	N_2/29	83	-	CO_2, Alkane	75/-	S10
Pt-KHT/28	water	-	250/4	N_2/45	83	-	CO_2, Alkane	67.4/-	S11
1Pt-3Ni/MWCNT	water	-	250	-/40	99	-	CO, CO_2, CH_4	90.9/-	S12
PtFe/ γ-Al_2O_3	water	-	225/-	-/27.6	66	-	CO, CO_2, CH_4	45.8/-	S13
Pt/SiO_2	water	-	230/4	-/32	10.8	-	CO, CO_2, Alkane	71.8/-	S14
Ce-Sm-5Cu	water	-	400-750/6	-	80	-	CO, CO_2, CH_4	44-75/-	S15
Ru/Y_2O_3	water	-	600/24	-	>99	-	CO, CO_2, CH_4	90	S16
Ru/Al_2O_3	water	-	900	-	58	-	CO, CO_2, CH_4	42	S17
Ru/Al_2O_3	water	-	350-500	-/10	50	-	CO, CO_2, CH_4	58.3	S18
Ru/Al_2O_3	water	-	400-600	-	92	-	CO, CO_2, CH_4	68	S19
Pt/ZrO_2	water	NaOH (1.5)	160/4.5	N_2/20	96	95	n. d.	-	S20
Ru-Zn-Cu(I)/HAP	water	NaOH (1.5)	100/12 120/12 140/12 140/21	vacuum vacuum vacuum vacuum	26.7 42.2 72.8 100	80.1 81.8 83.6 82.7	CH_4		S21
Pt-Co/CeO_x	water	NaOH (1.0)	200/4	N_2/10	85	88	CO_2, CH_4	-	S22
Au/HAP/BN	water	NaOH (1.0)	100/2	Air/1	100	99.5	n. d.	-	S23
Pt/C	water	NaOH (1.17)	140/3	C_2H_4/60	~100	95	n. d.	-	S24
Pt/C	water	NaOH (1.8)	180/24	He/30	100	80	n. d.	-	S25

Pt/C	-	KOH (1.1)	160/18	N_2/1	95	93	n. d.	-	S26
PtRu/C	water	NaOH (0.8)	200/1.5	H_2/40	100	37	CO_2, CH_4	-	S27
Pd/HAP	water	NaOH (1.1)	230/1.5	-	99	95	n. d.	-	S28
Rh/ZnO	water	NaOH (0.8)	180/12	He/20	~100	68	n. d.	-	S29
CuPd/rGO	water	NaOH (1.1)	140/6	N_2/14	56	88	n. d.	-	S30
Cu/SiO_2	water	NaOH (1.1-1.5)	240/6	N_2/14	75	82	CO_2, Alkanes	-	S31
CuO/CeO_2	water	NaOH (1.0)	220/8	N_2/20	87	74	n. d.	-	S32
$Ni_{0.3}$/graphite	water	NaOH (1.1)	230/2	N_2/1	97	92	n. d.	-	S33

NMC – N-doped mesoporous carbon, NaY – sodium zeolite, KHT – K-promoted hydrotalcite, MWCNT – multiwalled carbon nanotubes, HAP- hydroxyapatite, BN- boron nitride, rGO – reduced graphene oxide, n. d. – not determined

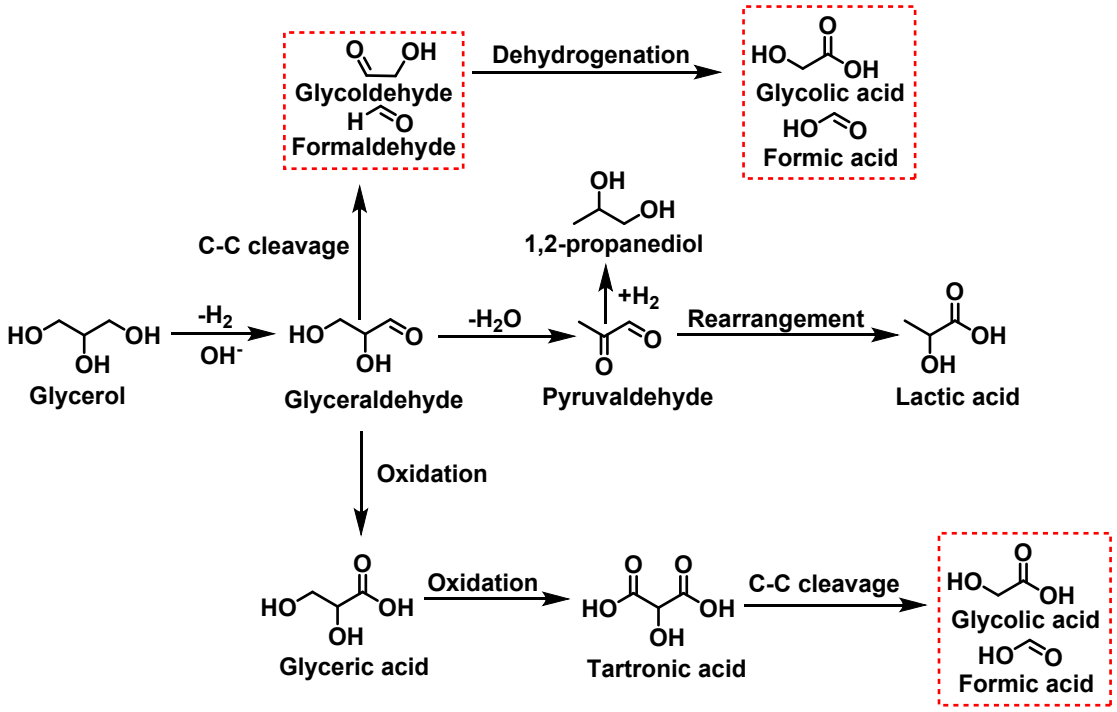

Scheme S1 Possible pathways for the catalytic conversion of GLY to H_2 gas and valuable co-products.

$$\underset{\text{Glycerol}}{C_3H_8O_3} \longrightarrow \underset{\text{Lactic acid}}{C_3H_6O_3} + H_2 \qquad ...(1)$$

$$\underset{\text{Glycerol}}{C_3H_8O_3} + 3H_2O \longrightarrow \underset{\text{Formic acid}}{3HCOOH} + 4H_2 \qquad ...(2)$$

Scheme S2 Key reactions involved in the transformation of glycerol to H_2 gas.

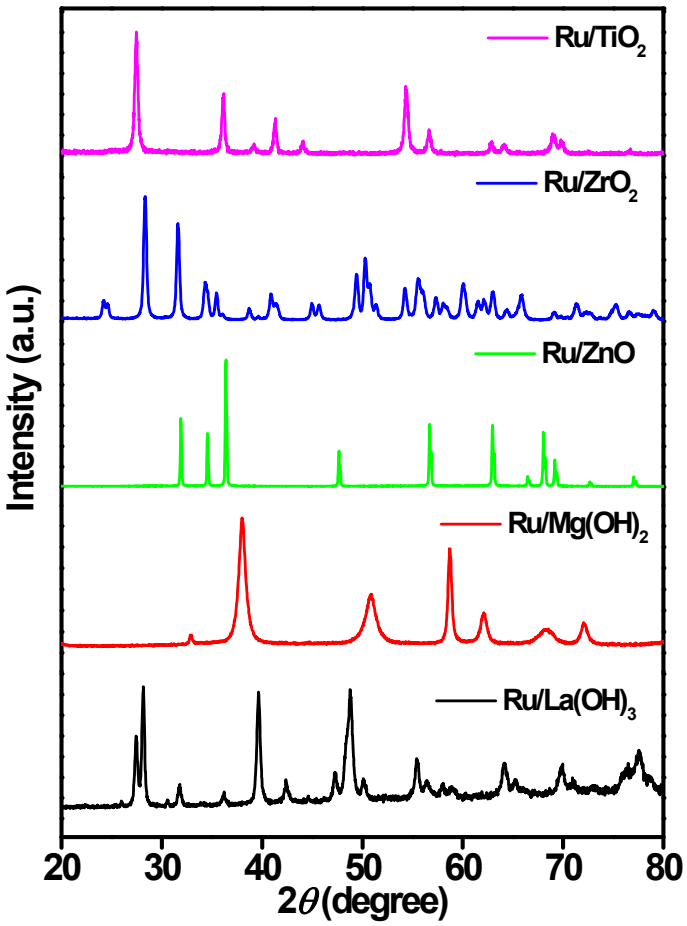

Fig. S1 P-XRD pattern of the ruthenium-based supported catalysts.

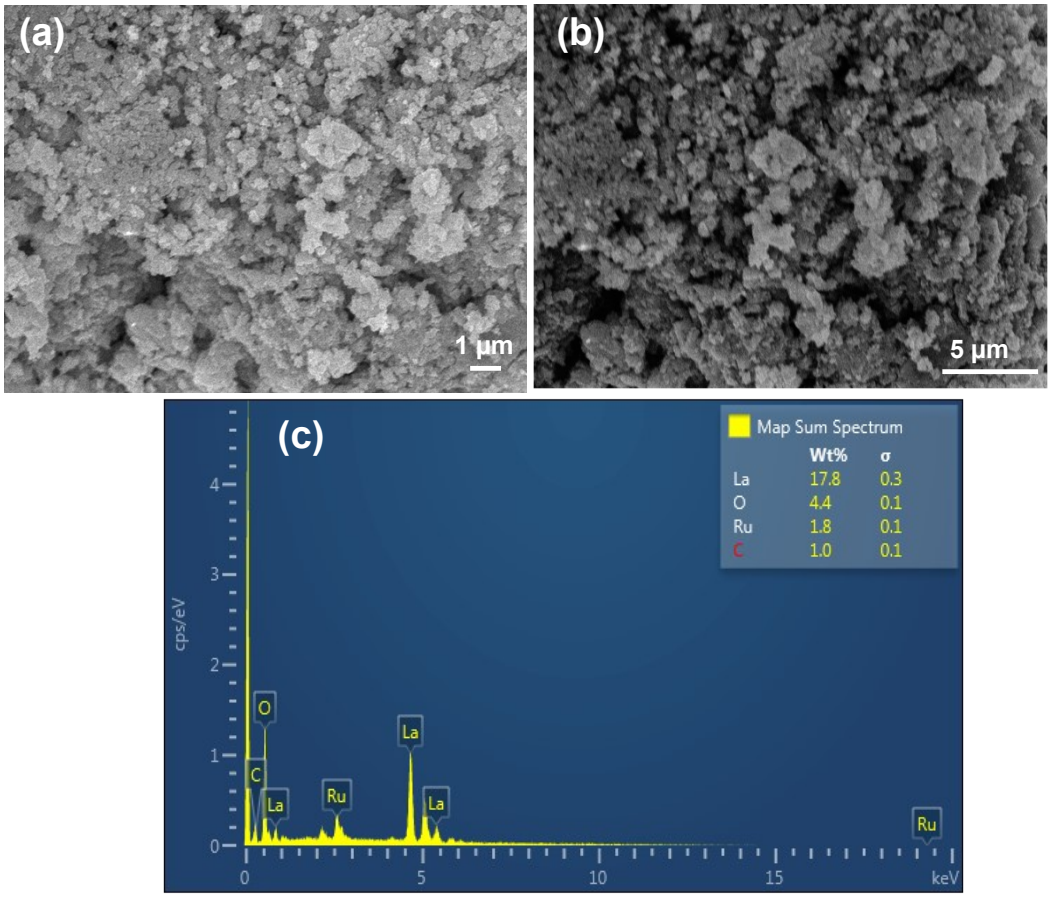

Fig. S2 (a-b) SEM images and (c) corresponding EDX spectra of Ru/La(OH)$_3$ catalyst.

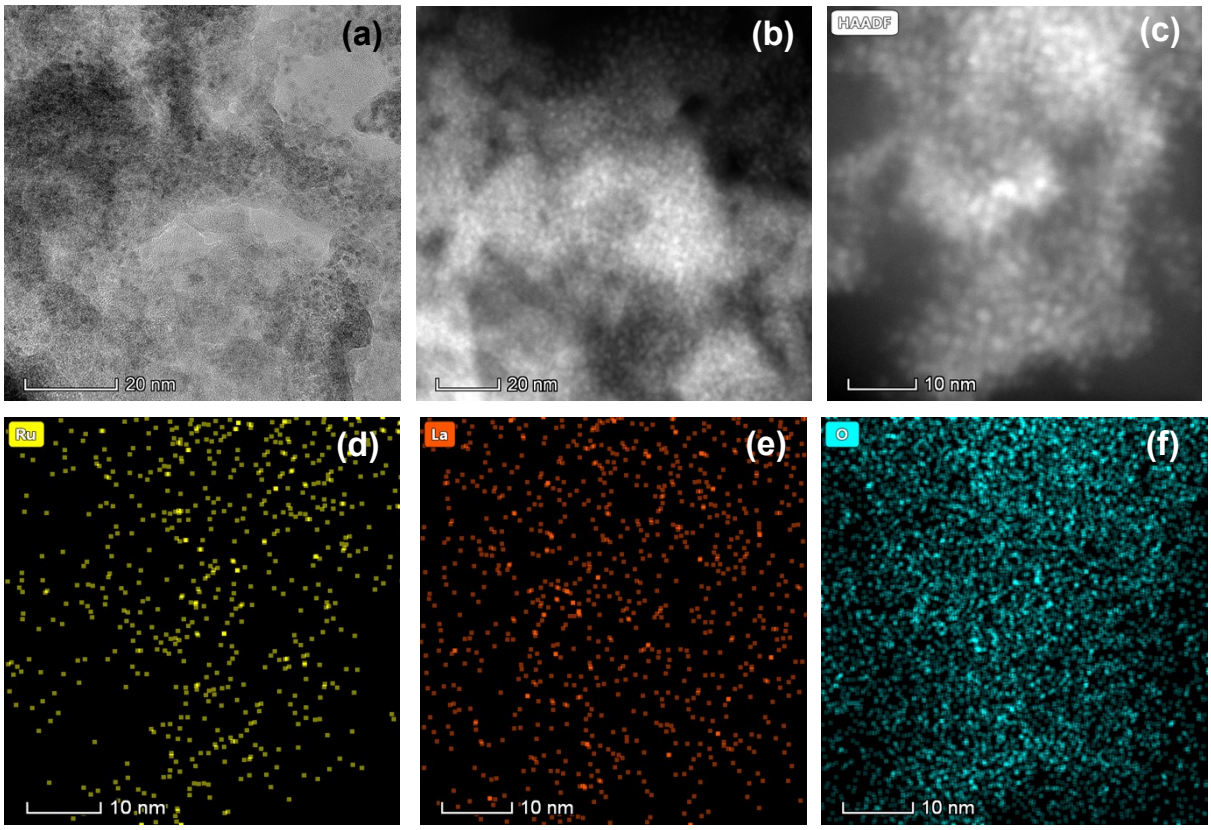

Fig. S3 (a) HR-TEM, (b-c) HAADF-STEM images and corresponding EDS elemental map of elements (d) Ruthenium (dark yellow), (e) Lanthanum (orange) and (f) Oxygen (cyan) of Ru/La$(OH)_3$ catalyst.

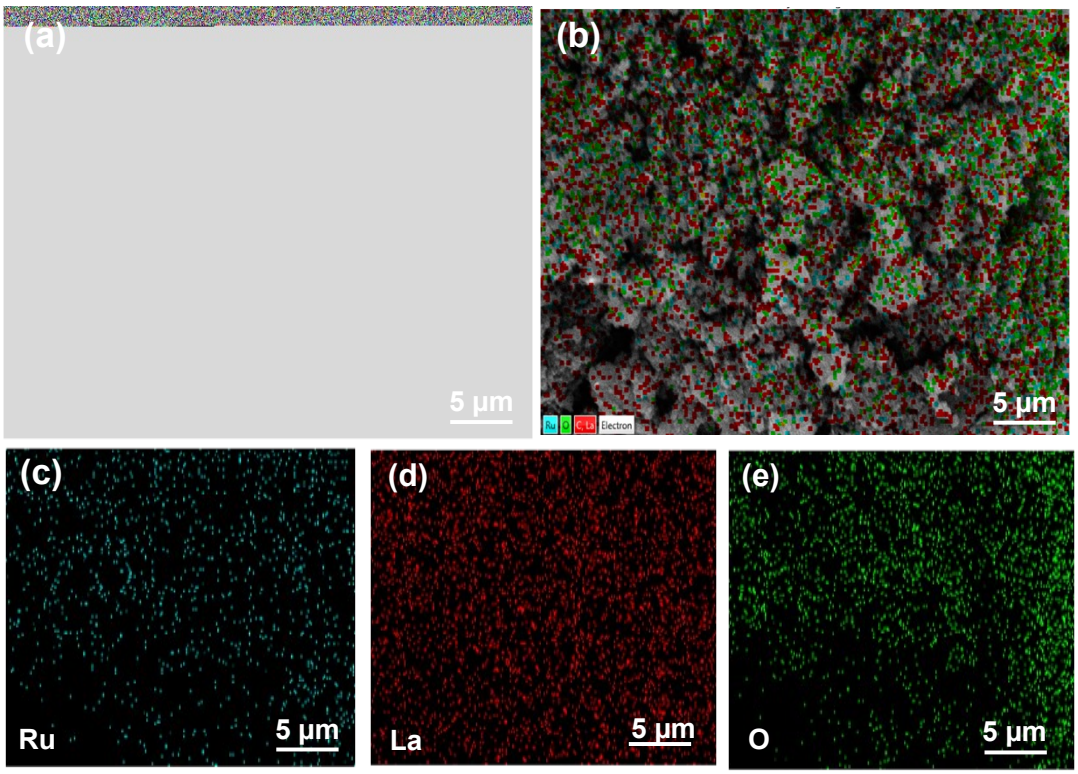

Fig. S4 (a) SEM image and (b) corresponding elemental mapping showing the presence of (c) Ru (cyan), (d) La (red), and (e) O (green) in the Ru/La$(OH)_3$ catalyst.

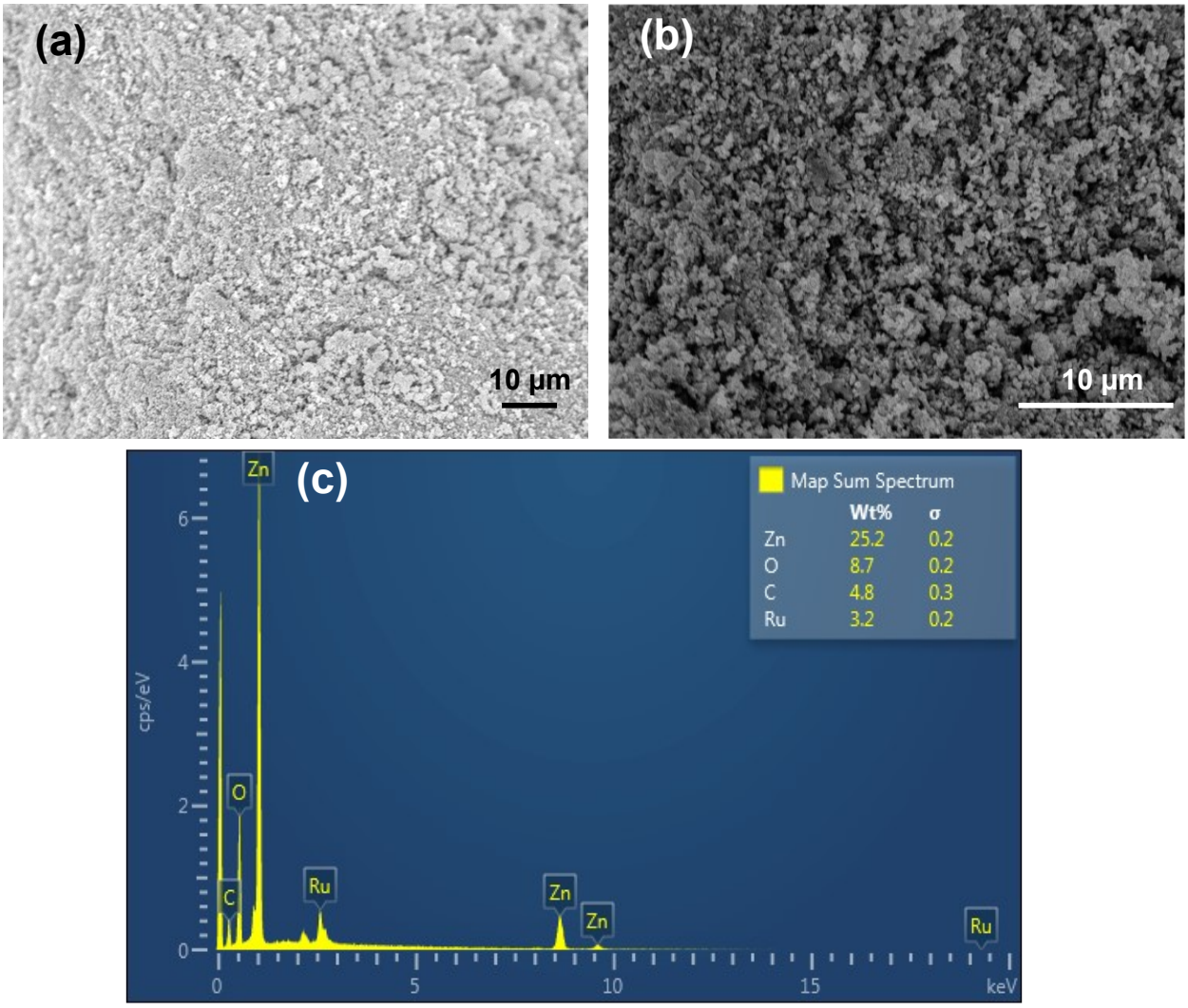

Fig. S5 (a-b) SEM images and (c) corresponding EDX spectra of Ru/ZnO catalyst.

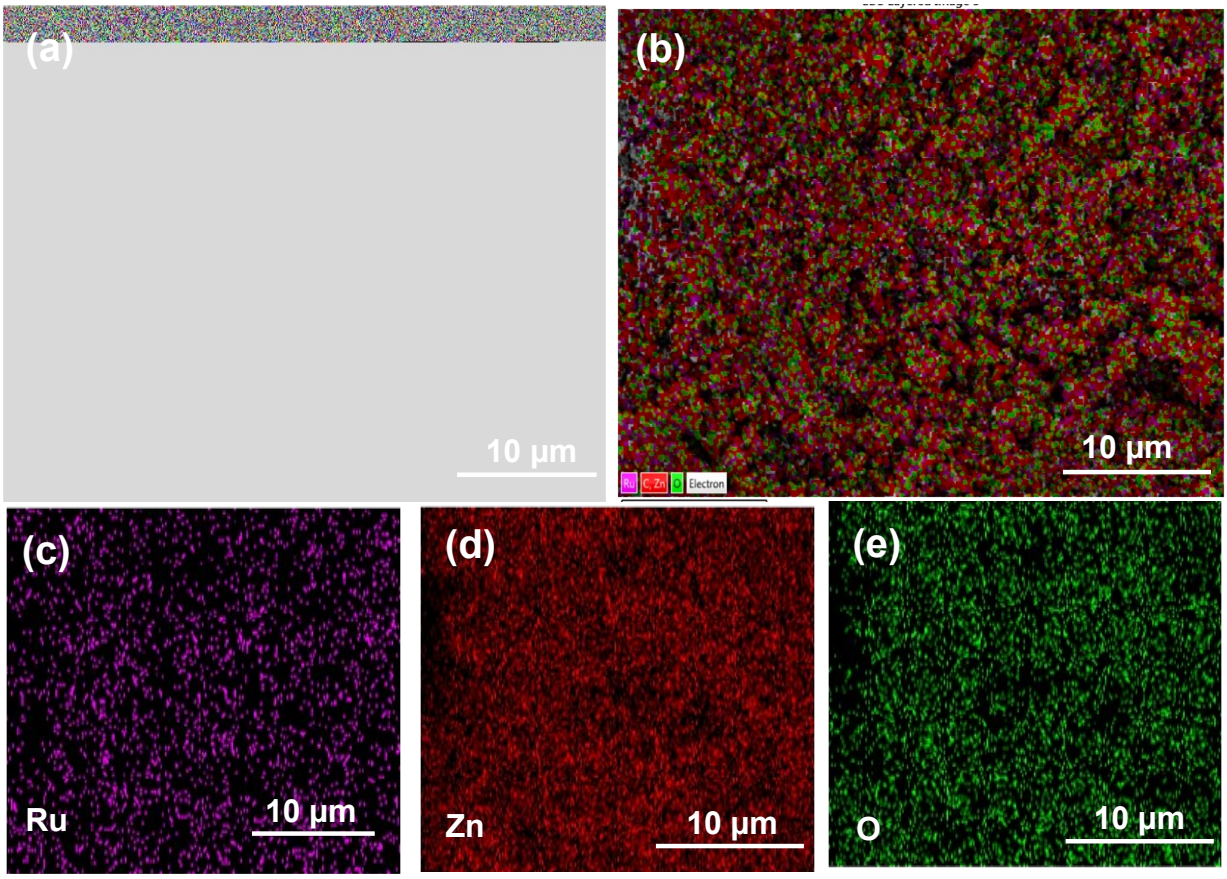

Fig. S6 (a) SEM image and (b) corresponding elemental mapping showing the presence of (c) Ru (purple), (d) Zn (red), and (e) O (green) in the Ru/ZnO catalyst.

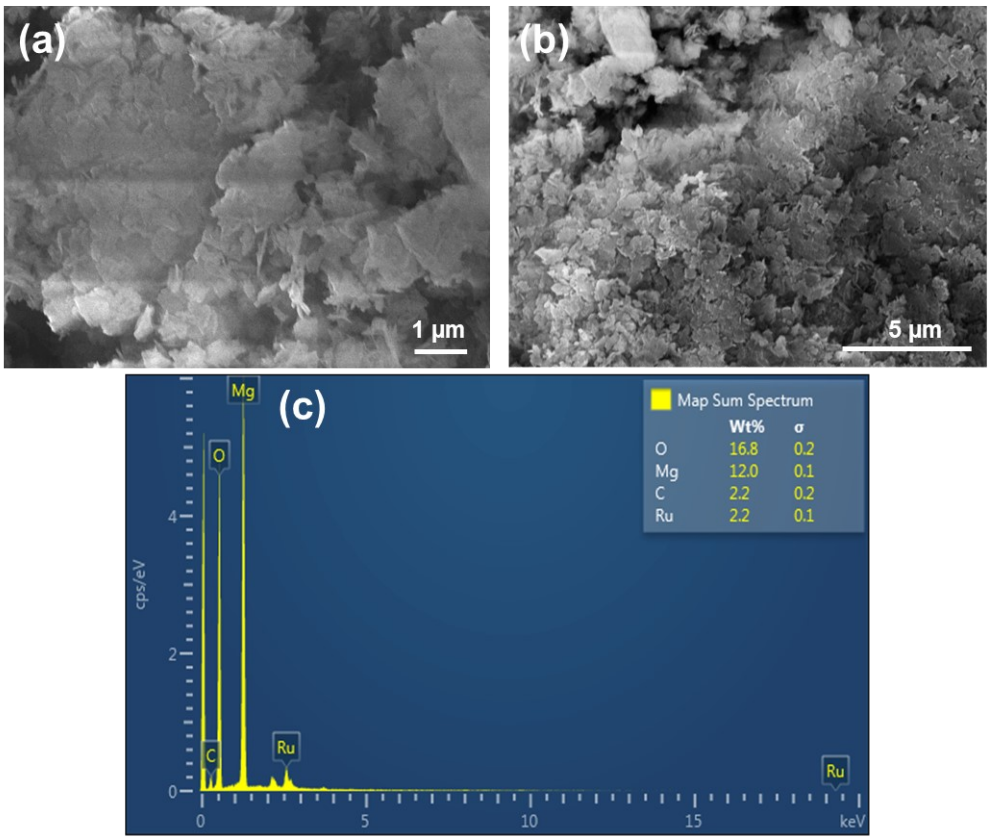

Fig. S7 (a-b) SEM images and (c) corresponding EDX spectra of Ru/$Mg(OH)_2$ catalyst.

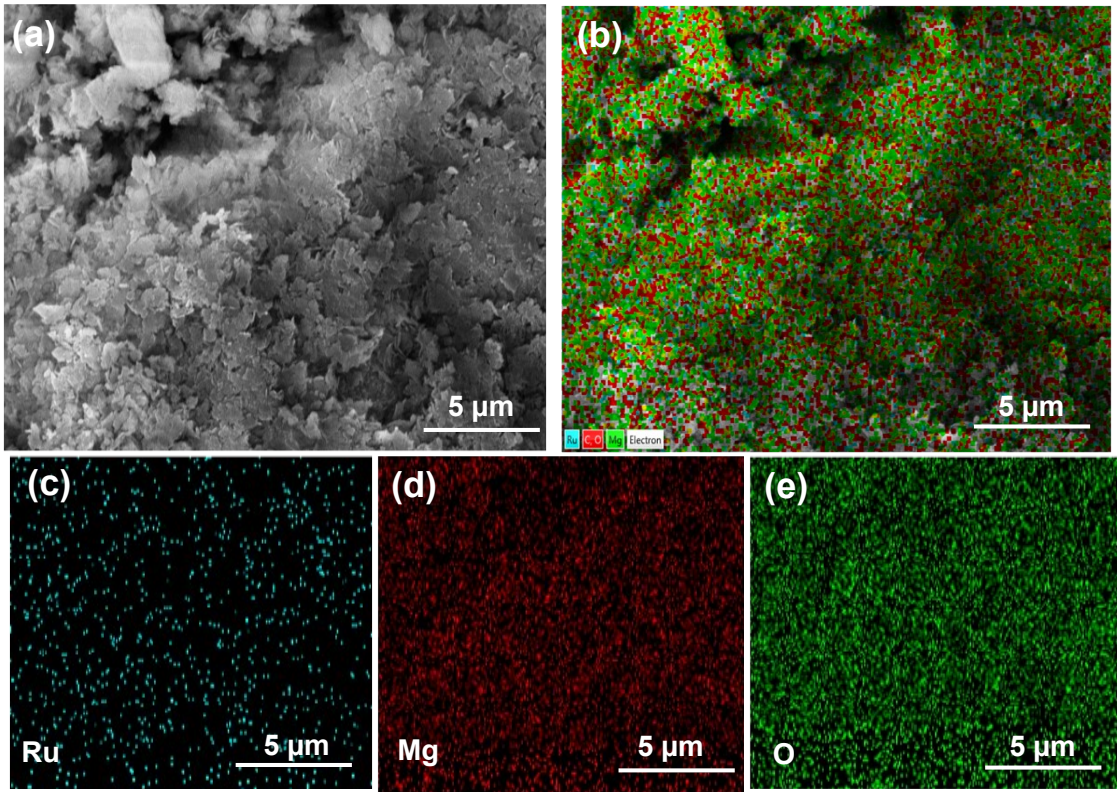

Fig. S8 (a) SEM image and (b) corresponding elemental mapping showing the presence of (c) Ru (cyan), (d) Mg (red), and (e) O (green) in Ru/$Mg(OH)_2$ catalyst.

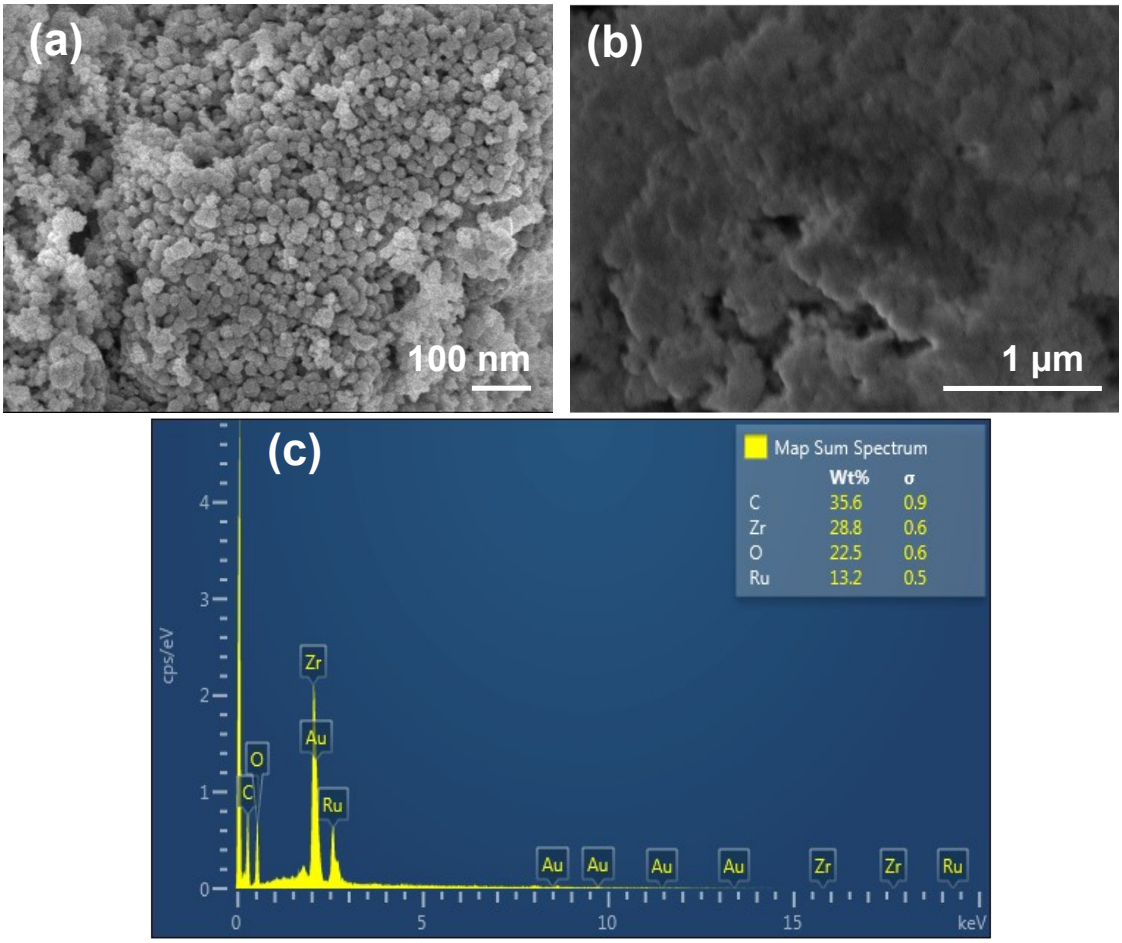

Fig. S9 (a-b) SEM images and (c) corresponding EDX spectra of Ru/ZrO_2 catalyst.

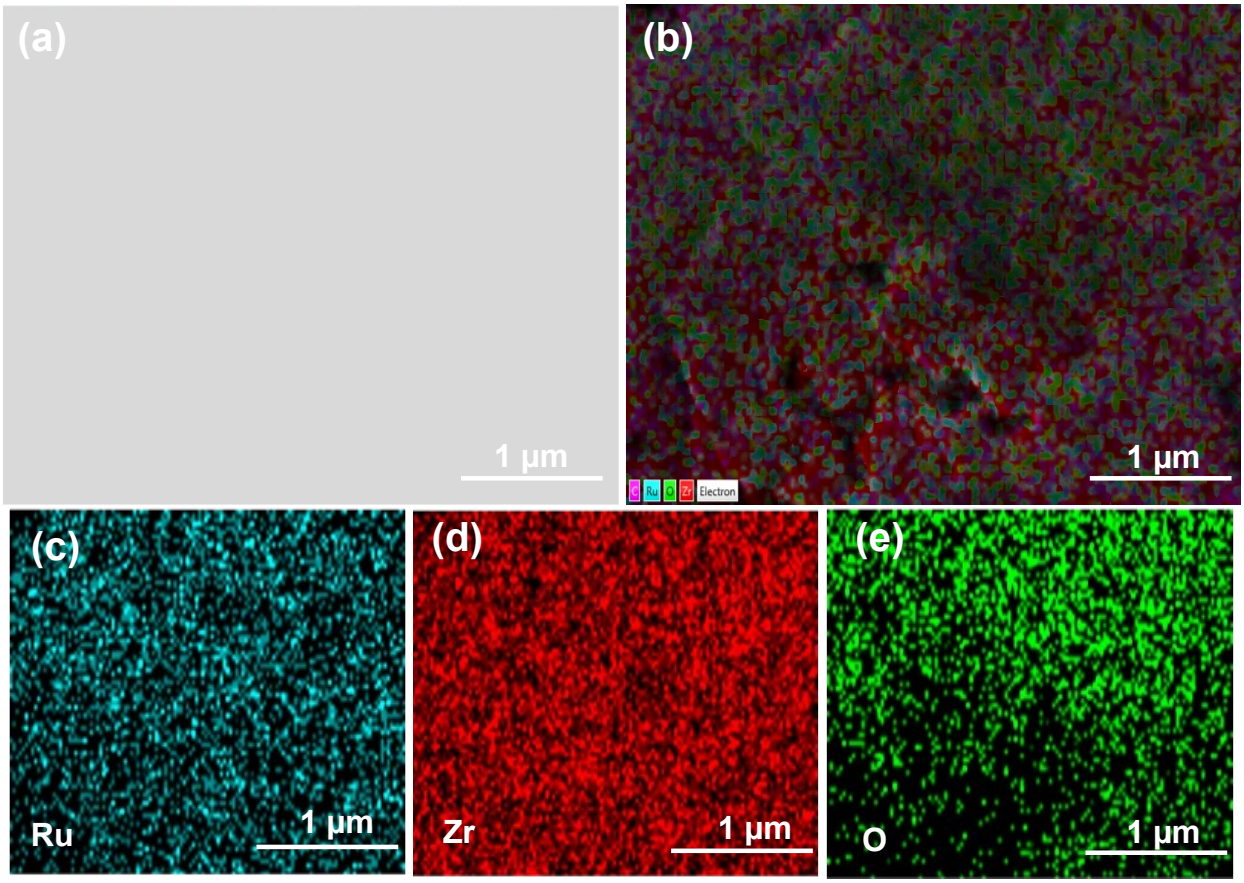

Fig. S10 (a) SEM image and (b) corresponding elemental mapping showing the presence of (c) Ru (cyan), (d) Zr (red), and (e) O (green) in Ru/ZrO_2 catalyst.

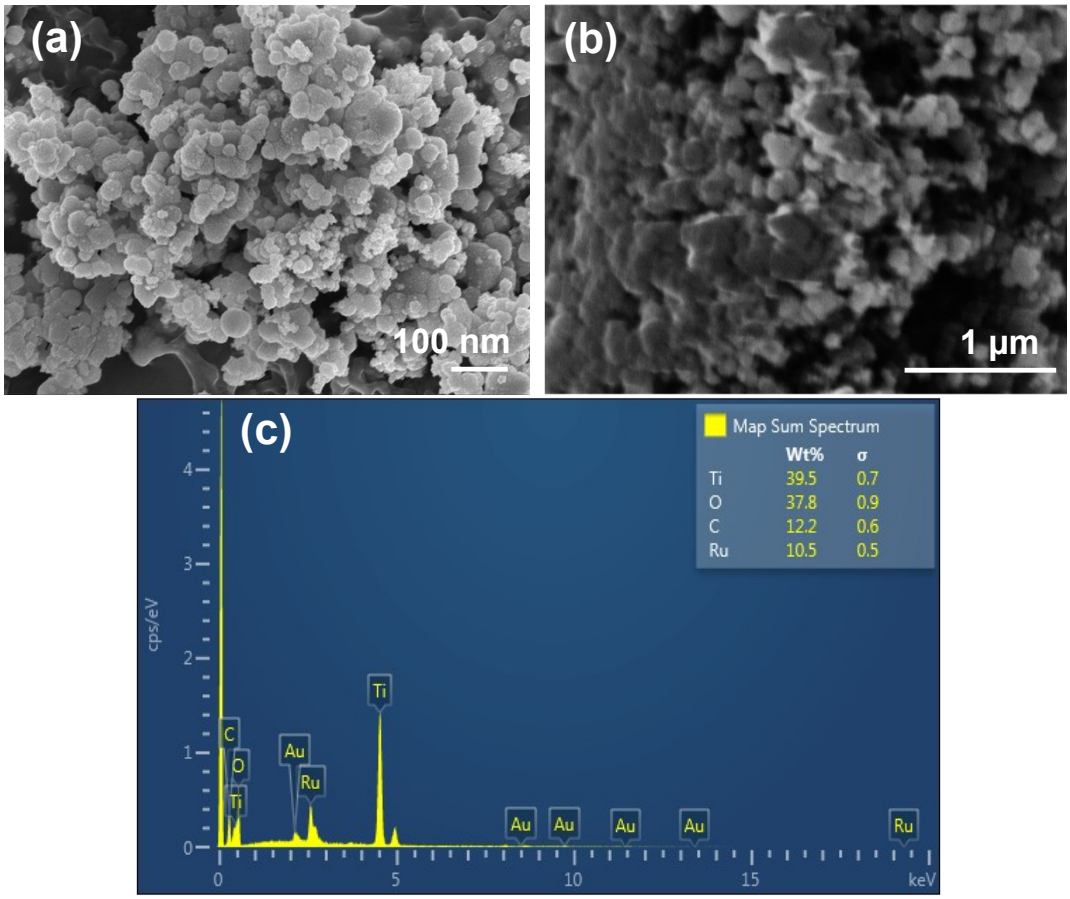

Fig. S11 (a-b) SEM images and (c) corresponding EDX spectra of Ru/TiO_2 catalyst.

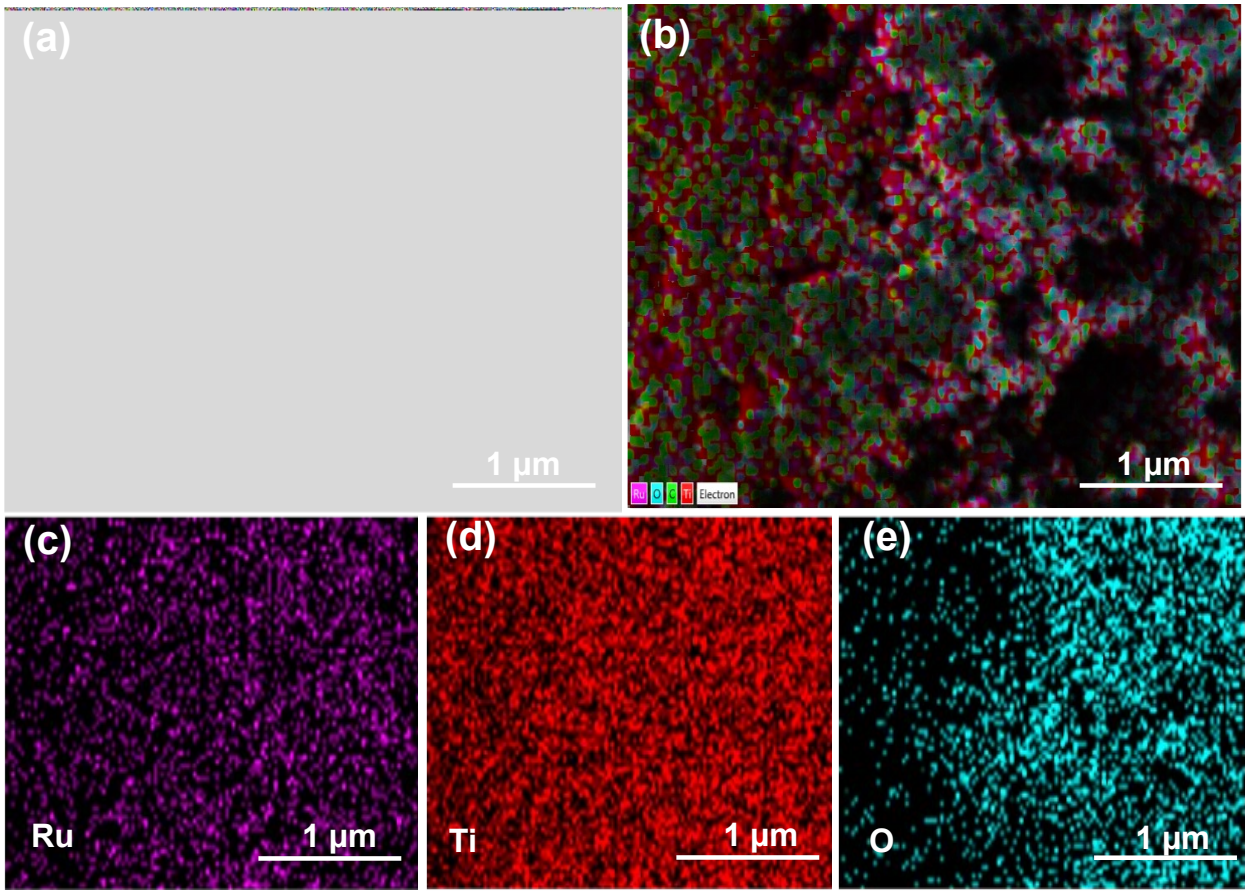

Fig. S12 (a) SEM image and (b) corresponding elemental mapping showing the presence of (c) Ru (purple), (d) Ti (red), and (e) O (cyan) in Ru/TiO_2 catalyst

Table S2. Textural properties of supported Ru catalysts.

Entry	Catalyst	Specific surface area (m^2/g)[a]	Metal loading (wt. %)[b]	Metal particle size (nm)[c]	Metal dispersion (%)[d]
1	$Ru/La(OH)_3$	81	9.0	1.5	87
2	Ru/ZnO	30	8.2	1.5	87
3	$Ru/Mg(OH)_2$	172	7.5	1.7	76
4	Ru/ZrO_2	30	8.3	1.8	72
5	Ru/TiO_2	27	8.6	1.5	87

[a]Calculated using N_2 adsorption-desorption isotherms. [b]Calculated using ICP-AES. [c]Particle size was calculated by TEM analysis. [d]Dispersion was calculated using the equation described in Ref. S3.

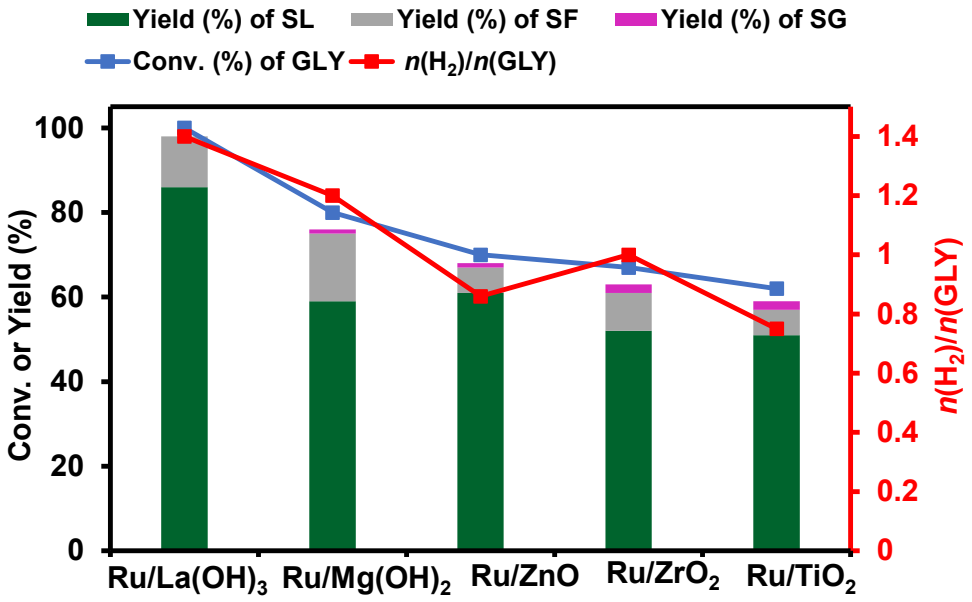

Fig. S13 Effect of different supports on the dehydrogenation of GLY to H_2 gas and SL. Reaction Conditions: Ru/support (100 mg), GLY (13.68 mmol), NaOH (27.36 mmol), water (41.04 mmol), 130 °C, 4.5 h, and 600 rpm.

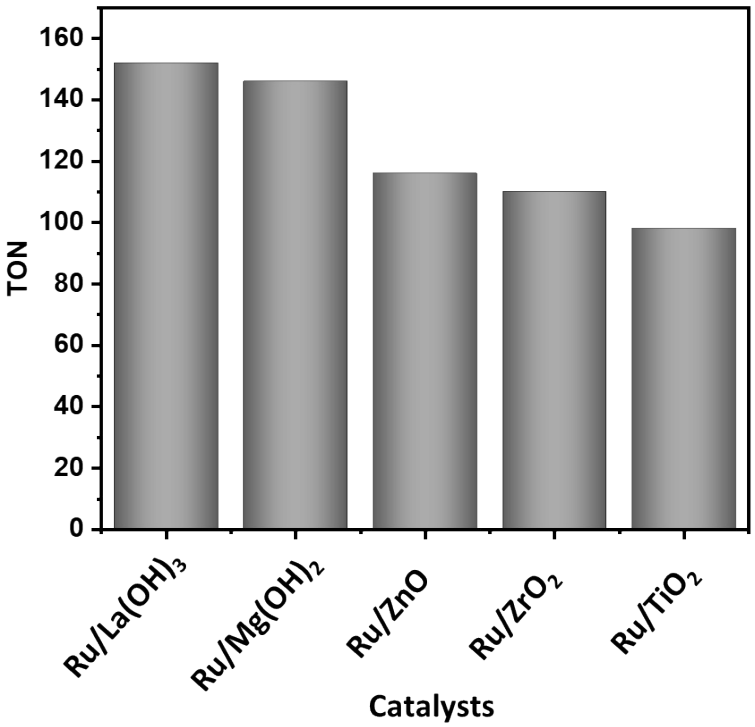

Fig. S14 Effect of different supports in the turnover number (TON) on the dehydrogenation of GLY to H_2 gas and SL. Reaction Conditions: Ru/support (100 mg), GLY (13.68 mmol), NaOH (27.36 mmol), water (41.04 mmol), 130 °C, 4.5 h, and 600 rpm.

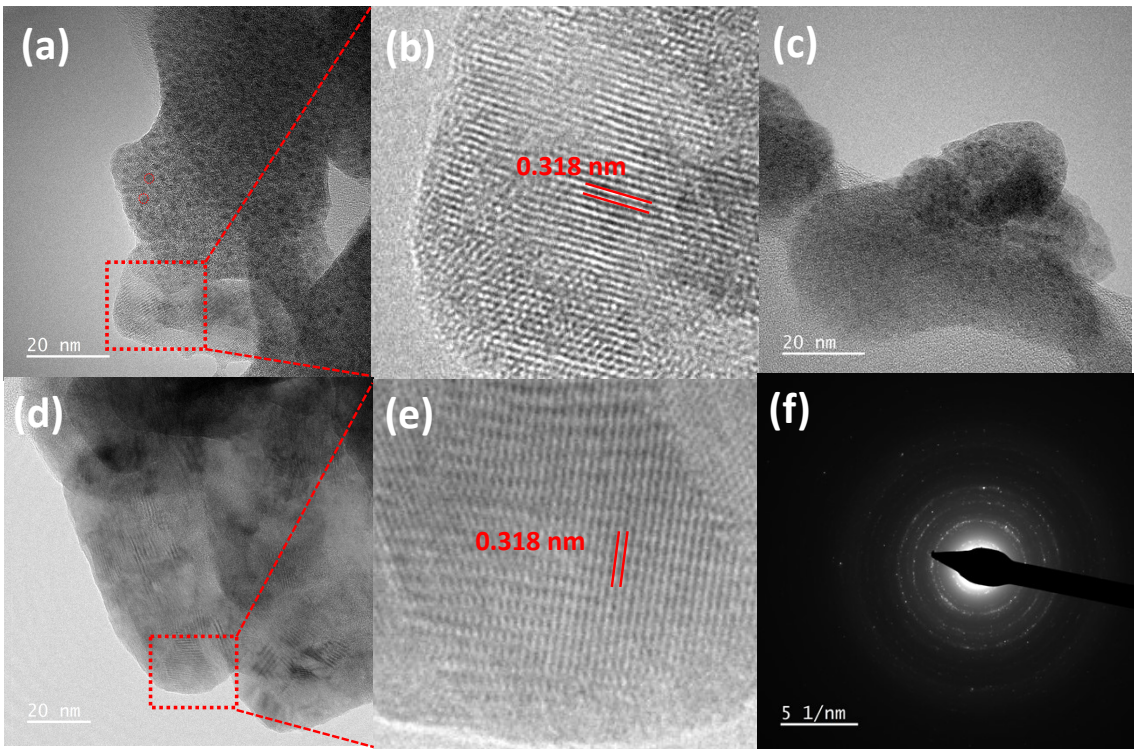

Fig. S15 TEM image of (a-c) Ru/La(OH)$_3$ catalyst, and red circled dark spot represent the Ru nanoparticles, (b) lattice fringes corresponding to La(OH)$_3$ support in Ru/La(OH)$_3$ catalyst, (d) La(OH)$_3$ support alone, (e) lattice fringes corresponding to Fig. (d), and (f) SAED pattern of La(OH)$_3$ support.

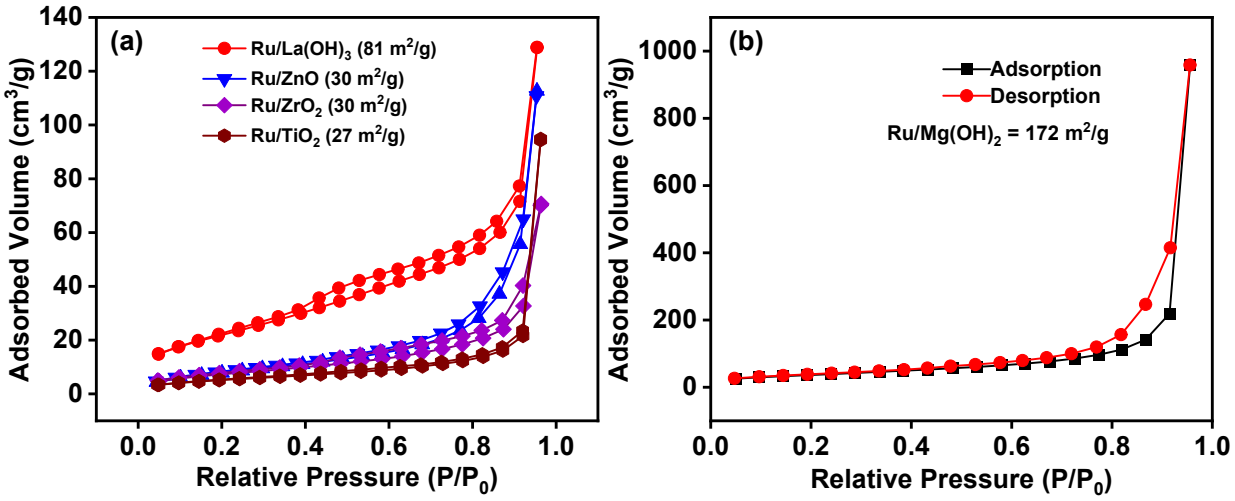

Fig. S16 N_2 adsorption-desorption isotherm of (a) Ru-supported catalysts and (b) Ru/Mg(OH)$_2$ catalyst.

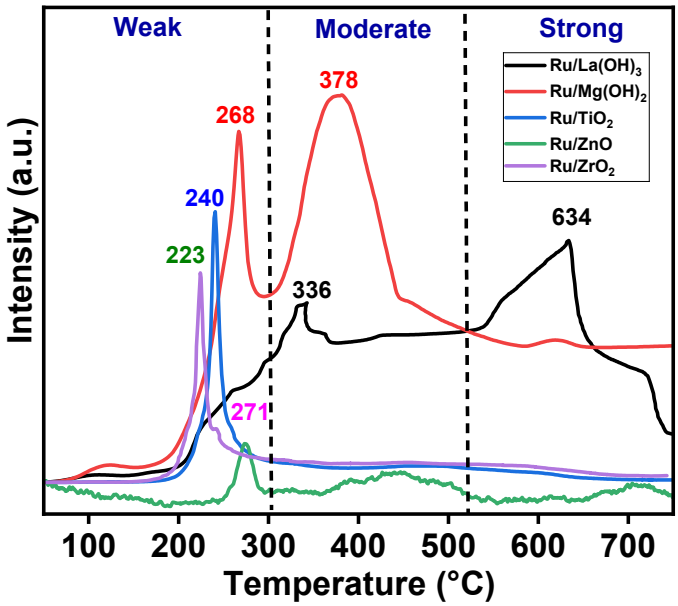

Fig. S17 CO_2 TPD profiles for supported Ru catalysts.

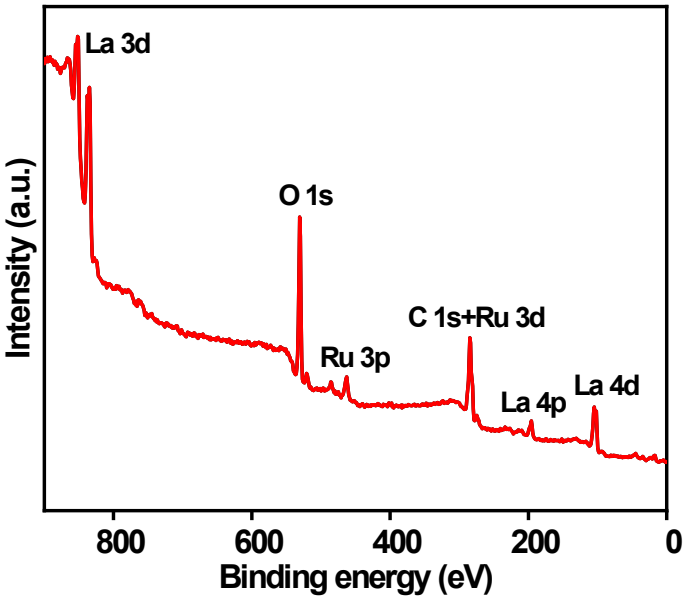

Fig. S18 Wide scan XPS spectra of the $Ru/La(OH)_3$ catalyst.

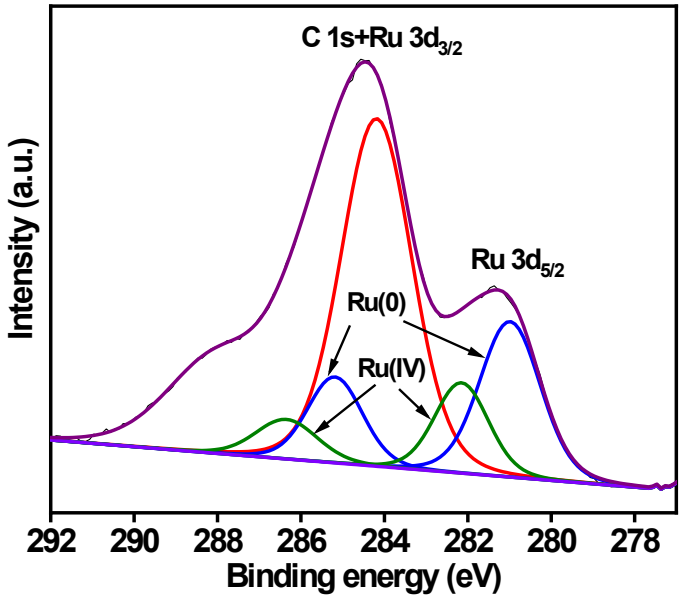

Fig. S19 XPS spectra of the Ru 3d region of the Ru/La(OH)$_3$ catalyst.

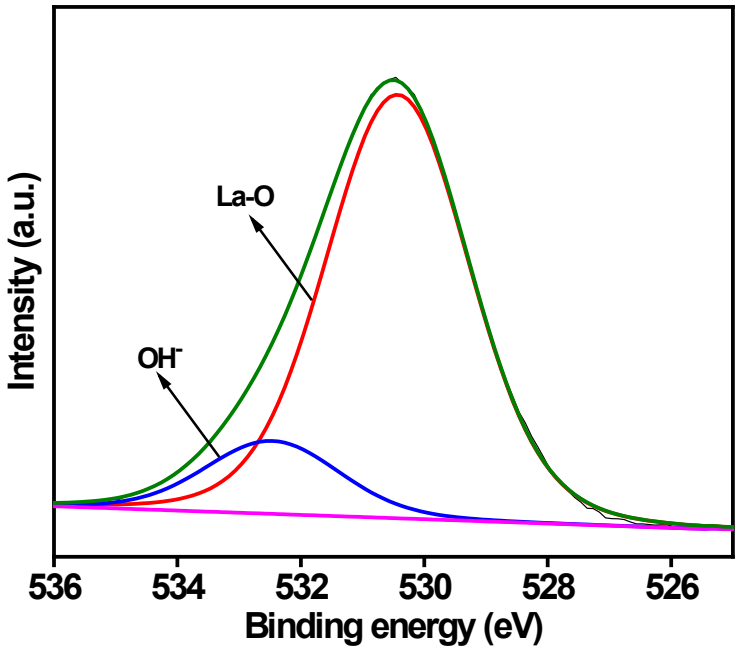

Fig. S20 XPS spectra of the O 1s region of the Ru/La(OH)$_3$ catalyst.

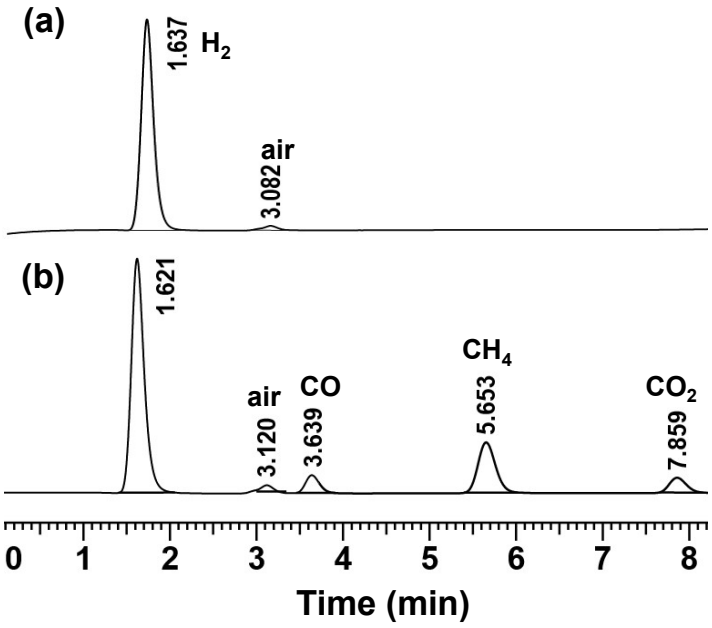

Fig. S21 (a) GC-TCD analysis of the gas produced from the reaction during dehydrogenation of glycerol and (b) standard mixture of gases with the composition of CO (24.965%), CO_2 (24.962%), CH_4 (25.012%), and H_2 (25.061%).

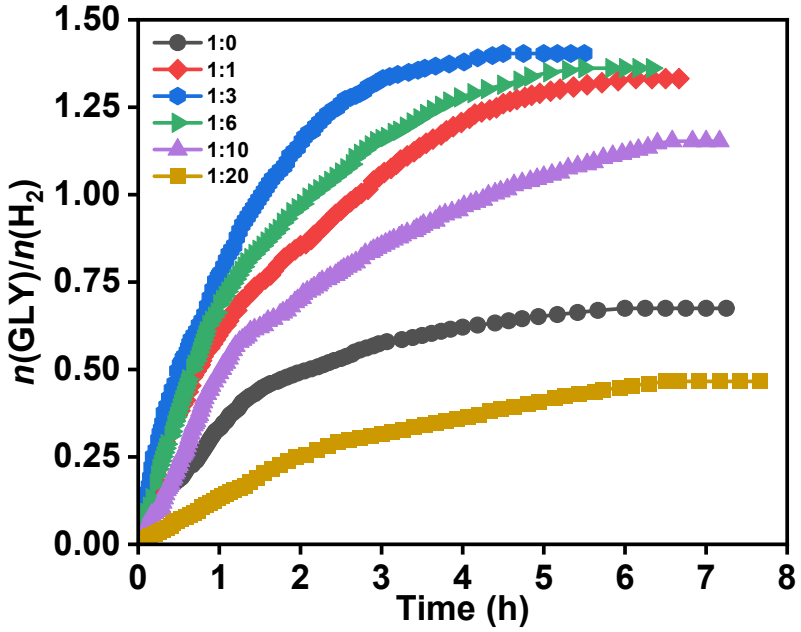

Fig. S22 Effect of water content: time course plot for hydrogen production from glycerol over the $Ru/La(OH)_3$ catalyst. Reaction conditions: $Ru/La(OH)_3$ (100 mg, 9 wt% Ru), glycerol (13.68 mmol), NaOH (27.36 mmol), water (0-20 equiv.), 130 °C, and 600 rpm.

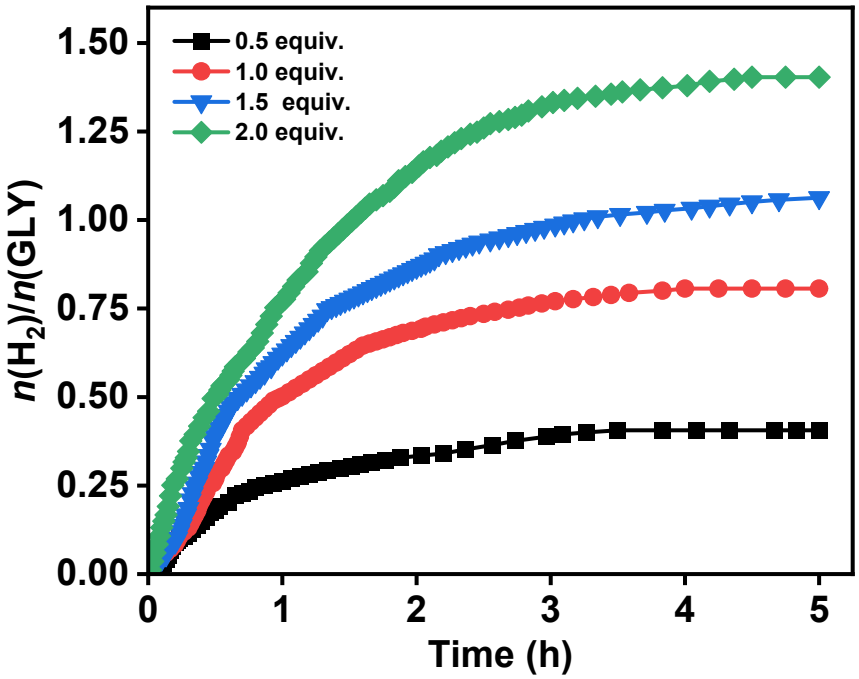

Fig. S23 Effect of base concentration: time course plot for hydrogen production from glycerol over the Ru/La(OH)$_3$ catalyst. Reaction conditions: Ru/La(OH)$_3$ (100 mg, 9 wt% Ru), glycerol (13.68 mmol), NaOH (0.5-2.0 equiv.), water (41.04 mmol), 130 °C, and 600 rpm.

Table S3 Effect of base and temperature in hydrogen production from glycerol over the $Ru/La(OH)_3$.[a]

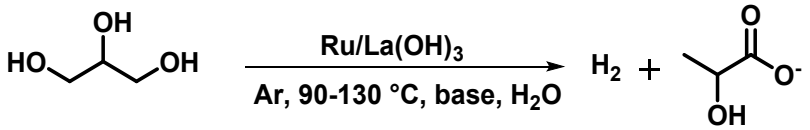

Entry	Base (2.0 equiv.)	T (°C) /t (h)	H_2 gas (mL)[b]	$n(H_2)/n$(GLY)	Conv. (%)	Yield of products (%)[c]				CB (%)[d]	Initial TOF (h^{-1})[e]
						SL (sel. %)	SG	PD	SF		
1	**NaOH**	**130/4.5**	**470**	**1.4**	**>99**	**86 (86)**	**-**	**-**	**12**	**98**	**105**
2	KOH	130/8	308	0.9	88	72 (82)	2	2	7	95	56
3	KO^{t}Bu	130/8	208	0.6	72	62 (86)	2	1	5	98	38
4	Na_2CO_3	130/4.5	-	-	n. r.	-	-		-	-	-
5	K_2CO_3	130/4.5	-	-	n. r.	-	-	-	-	-	-
6	NaOH	90/14	326	1.0	91	80 (88)	2	-	6	97	31
7	NaOH	100/12	360	1.1	95	85 (89)	1	-	6	97	41
8	NaOH	110/9	460	1.4	>99	87 (87)	-	-	11	98	57
9	NaOH	120/6.5	466	1.4	>99	86 (86)	1	-	10	97	77
10[f]	NaOH	130/8.5	88	0.3	52	41 (79)	2	-	5	96	10
11[g]	NaOH	130/10	144	0.4	70	56 (80)	3	-	6	95	21
12[h]	NaOH	130/6.5	354	1.1	95	79 (83)	2	-	11	97	52

[a]Reaction conditions: $Ru/La(OH)_3$ (100 mg, 9 wt% Ru), GLY (13.68 mmol), base (27.36 mmol), water (41.04 mmol), 90-130 °C and 600 rpm. [b]Volume of gas was measured by water displacement method. [c]Yield was calculated by ^{1}H NMR using sodium acetate as an internal standard. [d]CB is carbon balance. [e]Turnover frequency was calculated based on the volume of H_2 gas released in initial 1 h; TOF = TON/t. [f]$Ru/La(OH)_3$ catalyst (100 mg, 1 wt% Ru), [g]$Ru/La(OH)_3$ catalyst (100 mg, 2.5 wt% Ru), [h]$Ru/La(OH)_3$ catalyst (100 mg, 5 wt% Ru). The results reported are the average of at least two repeated reactions. SL (sodium lactate), SG (sodium glycolate), PD (1,2-propanediol), and SF (sodium formate). n. r. (no reaction)

Table S4. Recyclability data at the intermediate conversion of GLY.[a]

Sr. No.	Catalytic run	GLY conv. (%)	$n(H_2)$ /n(GLY)	Selectivity (yield) (%) on carbon basis			
				SL	**SG**	**PD**	**SF**
1	Run 1	62	0.45	87 (54)	3 (2)	2 (1)	6 (4)
2	Run 2	62	0.45	87 (54)	3 (2)	2 (1)	6 (4)
3	Run 3	62	0.45	87 (54)	3 (2)	2 (1)	6 (4)
4	Run 4	62	0.45	87 (54)	3 (2)	2 (1)	6 (4)
5	Run 5	62	0.45	87 (54)	3 (2)	2 (1)	6 (4)
6	Run 6	62	0.45	87 (54)	3 (2)	2 (1)	6 (4)
7	Run 7	60	0.43	88 (53)	2 (1)	2 (1)	3 (2)
8	Run 8	60	0.43	88 (53)	2 (1)	2 (1)	3 (2)
9	Run 9	58	0.41	86 (50)	2 (1)	2 (1)	3 (2)
10	Run 10	56	0.39	86 (48)	2 (1)	2 (1)	3 (3)

[a]Reaction conditions: Ru/$La(OH)_3$ (100 mg, 9 wt% Ru), GLY (13.68 mmol), NaOH (27.36 mmol), water (41.04 mmol), 130 °C, 1.5 h, and 600 rpm.

Table S5. Recyclability data at the complete conversion of GLY.[a]

Sr. No.	Catalytic run	GLY conv. (%)	$n(H_2)$ /n(GLY)	Selectivity (yield) (%) on carbon basis			
				SL	**SG**	**PD**	**SF**
1	Run 1	>99	1.4	86 (86)	-	-	12 (12)
2	Run 2	>99	1.4	86 (86)	-	-	12 (12)
3	Run 3	>99	1.4	86 (86)	-	-	12 (12)
4	Run 4	>99	1.4	86 (86)	-	-	12 (12)
5	Run 5	>99	1.4	86 (86)	-	-	12 (12)
6	Run 6	96	1.34	85 (82)	2	1	6 (6)
7	Run 7	96	1.34	85 (82)	2	1	6 (6)
8	Run 8	92	1.3	85 (78)	2	1	6 (6)
9	Run 9	89	1.2	84 (75)	2	1	7 (6)
10	Run 10	88	1.17	84 (74)	2	2	7 (6)

[a]Reaction conditions: Ru/$La(OH)_3$ (100 mg, 9 wt% Ru), GLY (13.68 mmol), NaOH (27.36 mmol), water (41.04 mmol), 130 °C, and 600 rpm.

Table S6 Effect of stirring speed on the dehydrogenation of GLY over the $Ru/La(OH)_3$ catalyst.[a]

Entry	RPM	conv. (%)	t (h)	$n(H_2)$ /n(GLY)	Yield of byproducts (% C)[b]				CB	Average reaction rate ($mol/g_{Ru}/h \times 10^{-1}$)
					SL (sel. %)	SG	PD	SF		
1	-	91	6	1.1	75 (82)	3	2	7	96	2.07
2	200	93	6	1.3	78 (84)	4	1	7	97	2.12
3	400	>99	5	1.4	82 (82)	2	-	11	96	2.73
4	600	>99	4.5	1.4	86 (86)	-	-	12	98	3.04
5	800	>99	4.5	1.4	84 (84)	-	-	12	96	3.04

[a]Reaction conditions: $Ru/La(OH)_3$ (100 mg, 9 wt% Ru), GLY (13.68 mmol), NaOH (27.36 mmol), water (41.04 mmol), 130 °C. [b]Yield was calculated by ^1H NMR using sodium acetate as an internal standard. CB is carbon balance.

Mass transfer limitations: It has been observed that the GLY conversion and the selectivity for H_2 and SL increased linearly with the increase in stirring speed up to 600 rpm but does not change significantly for stirring speed ≥ 600 rpm, suggesting that external mass transfer limitations are not applicable for the stirring speed of ≥ 600 rpm.[S34-S35]

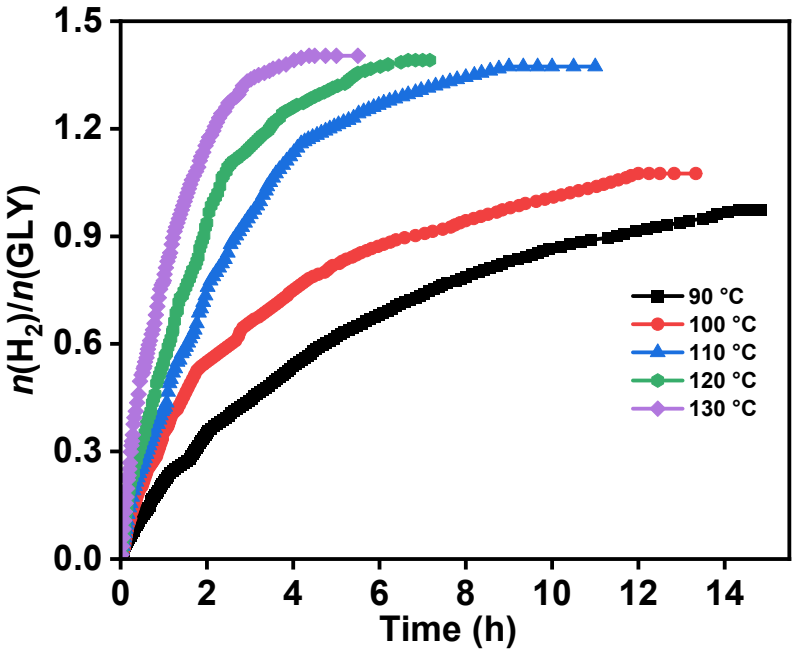

Fig. S24 Effect of temperature in hydrogen production from glycerol over the Ru/La(OH)$_3$ catalyst. Reaction conditions: Ru/La(OH)$_3$ (100 mg, 9 wt% Ru), glycerol (13.68 mmol), NaOH (27.36 mmol), water (41.04 mmol), 90-130 °C, and 600 rpm.

Arrhenius equation for the calculation of activation energy

$$k = Ae^{-Ea/RT}$$

$$\ln k = \ln A + (-E_a/RT),$$

where E_a is the activation energy, R is the molar gas constant (8.314 J/K/mol), and T is the temperature in Kelvin (363 K - 403 K).

(a)

Entry	T (K)	1/Tx10^3 (K^{-1})	H_2 (mL) in 1 h	TOF (h^{-1})	lnTOF (h^{-1})
1	363	2.7548	76	31.0457	3.4354
2	373	2.6809	100	40.8496	3.7098
3	383	2.6109	140	57.1895	4.0463
4	393	2.5445	190	77.6143	4.3517
5	403	2.4813	258	105.3921	4.6576

(b)

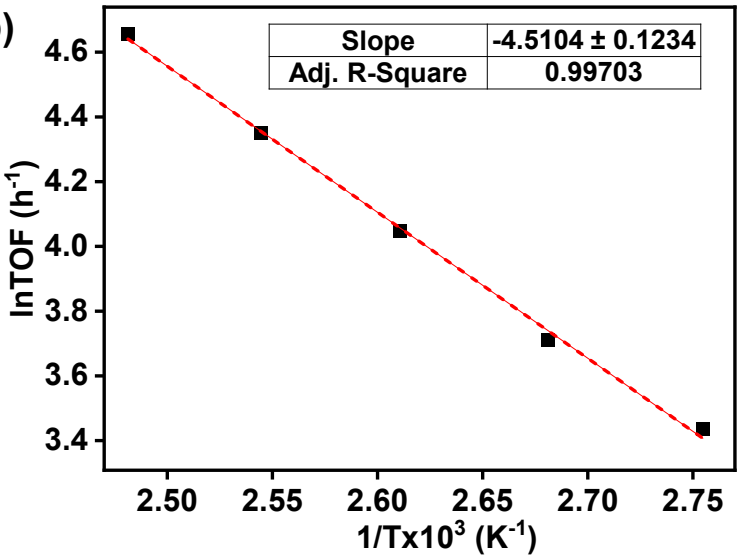

Fig. S25 (a) Data table for calculation of activation energy (b) Arrhenius plot of initial TOF values (1 h). Reaction conditions: Ru/La(OH)$_3$ (100 mg, 9 wt% Ru), glycerol (13.68 mmol), NaOH (27.36 mmol), water (41.04 mmol), 90-130 °C, 1 h, and 600 rpm.

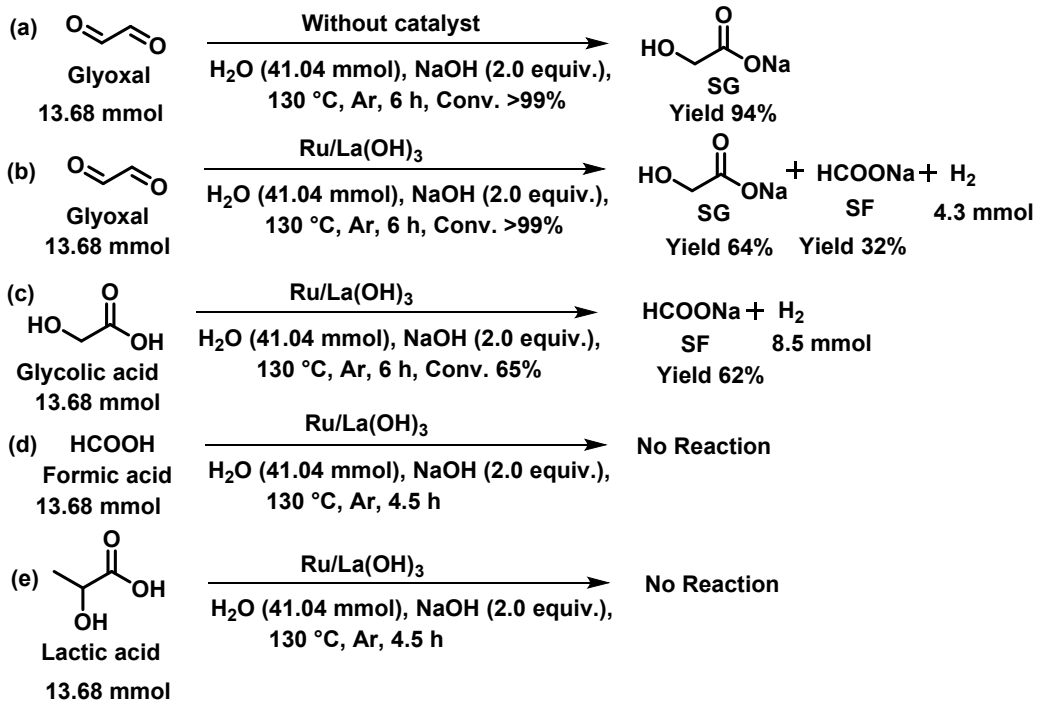

Scheme S3 Control experiments to elucidate the reaction intermediates in the catalytic transformation of GLY to H_2 and SL. (a) Catalytic reaction for hydrogen production from glyoxal without catalyst. Reaction conditions: Glyoxal (13.68 mmol), NaOH (27.36 mmol), water (41.04 mmol), 130 °C, and 600 rpm. Catalytic dehydrogenation from (b) glyoxal, (c) glycolic acid, (d) formic acid, and (e) lactic acid over the $Ru/La(OH)_3$ catalyst. Reaction conditions: Substrate (13.68 mmol), $Ru/La(OH)_3$ (100 mg, 9 wt% Ru), NaOH (27.36 mmol), water (41.04 mmol), 130 °C, and 600 rpm.

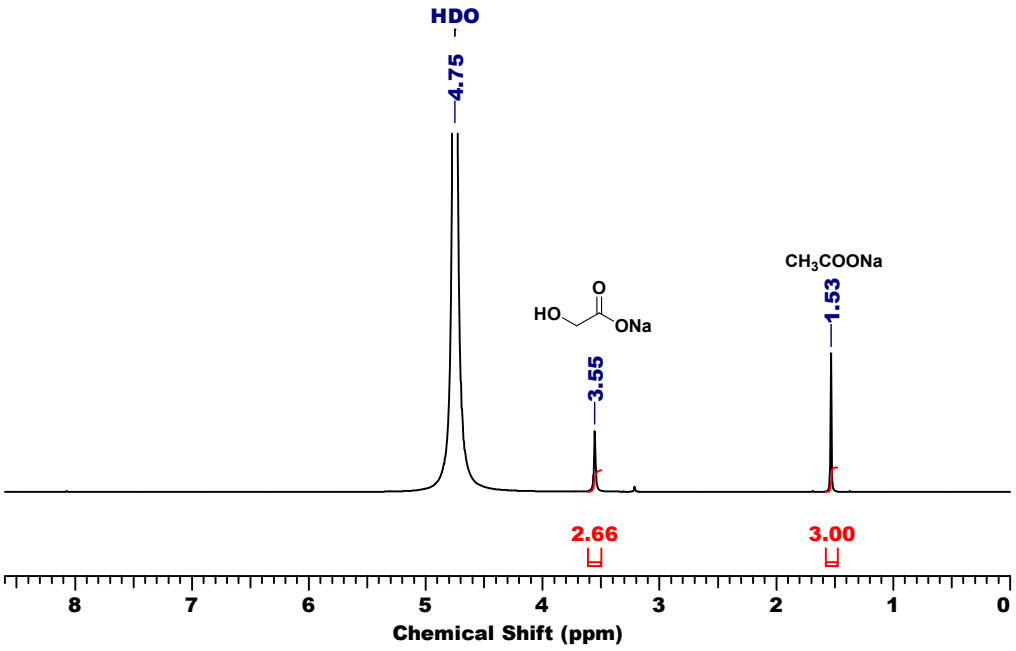

Fig. S26 ^{1}H NMR spectra of the crude reaction mixture of the catalytic reaction for hydrogen production from glyoxal without catalyst. Reaction conditions: glyoxal (13.68 mmol), NaOH (27.36 mmol), water (41.04 mmol), 130 °C, and 600 rpm.

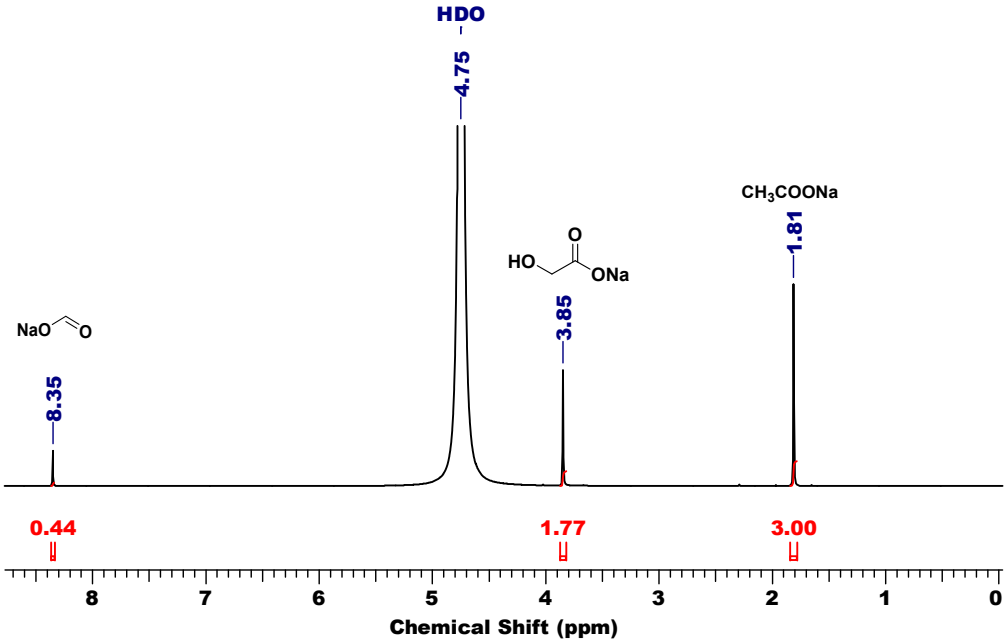

Fig. S27 ^{1}H NMR spectra of the crude reaction mixture of the catalytic reaction for hydrogen production from glyoxal over Ru/La(OH)$_3$ catalyst. Reaction conditions: Ru/La(OH)$_3$ (100 mg, 9 wt% Ru), glyoxal (13.68 mmol), NaOH (27.36 mmol), water (41.04 mmol), 130 °C, and 600 rpm.

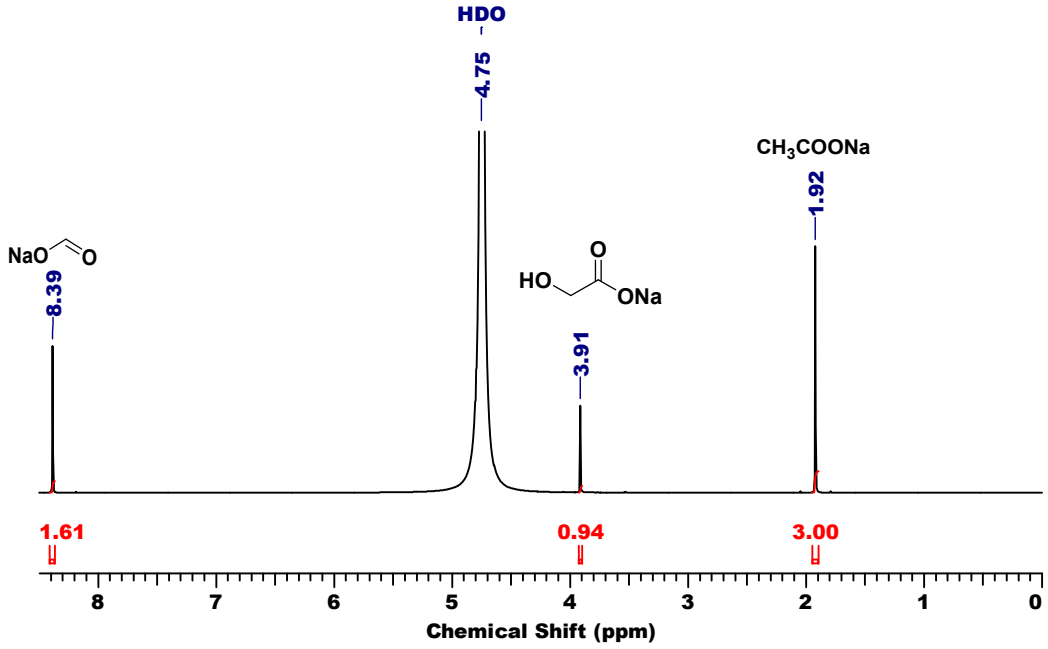

Fig. S28 ^{1}H NMR spectra of the crude reaction mixture of the catalytic reaction for hydrogen production from glycolic acid over Ru/La(OH)$_3$ catalyst. Reaction conditions: Ru/La(OH)$_3$ (100 mg, 9 wt% Ru), glycolic acid (13.68 mmol), NaOH (27.36 mmol), water (41.04 mmol), 130 °C, and 600 rpm.

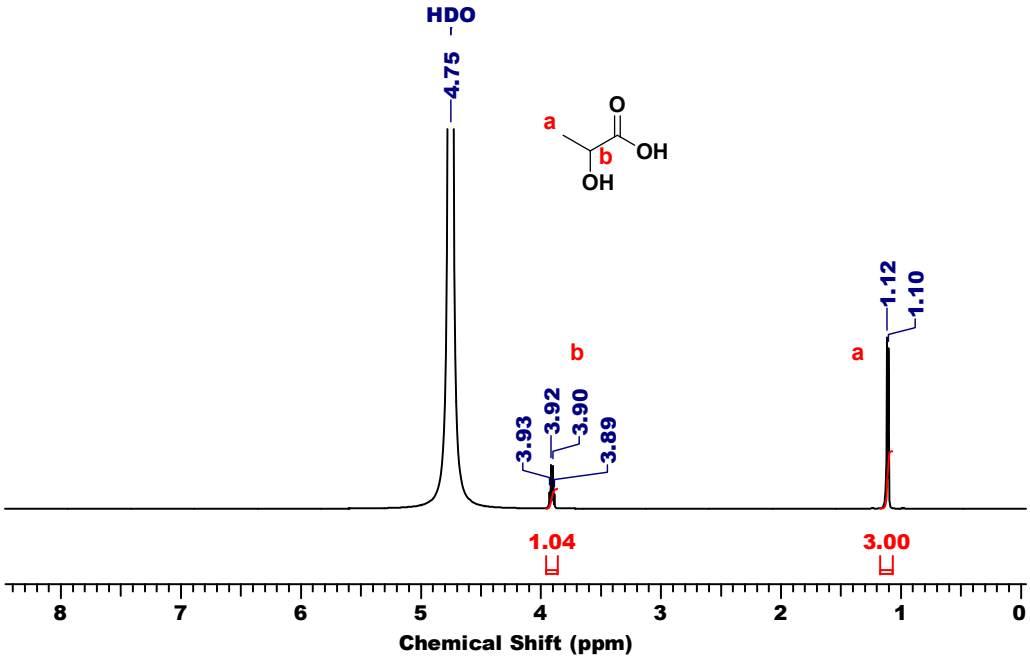

Fig. S29 ^{1}H NMR spectra of the crude reaction mixture of the catalytic reaction for hydrogen production from lactic acid over Ru/La(OH)$_3$ catalyst. Reaction conditions: Ru/La(OH)$_3$ (100 mg, 9 wt% Ru), lactic acid (13.68 mmol), NaOH (27.36 mmol), water (41.04 mmol), 130 °C, and 600 rpm.

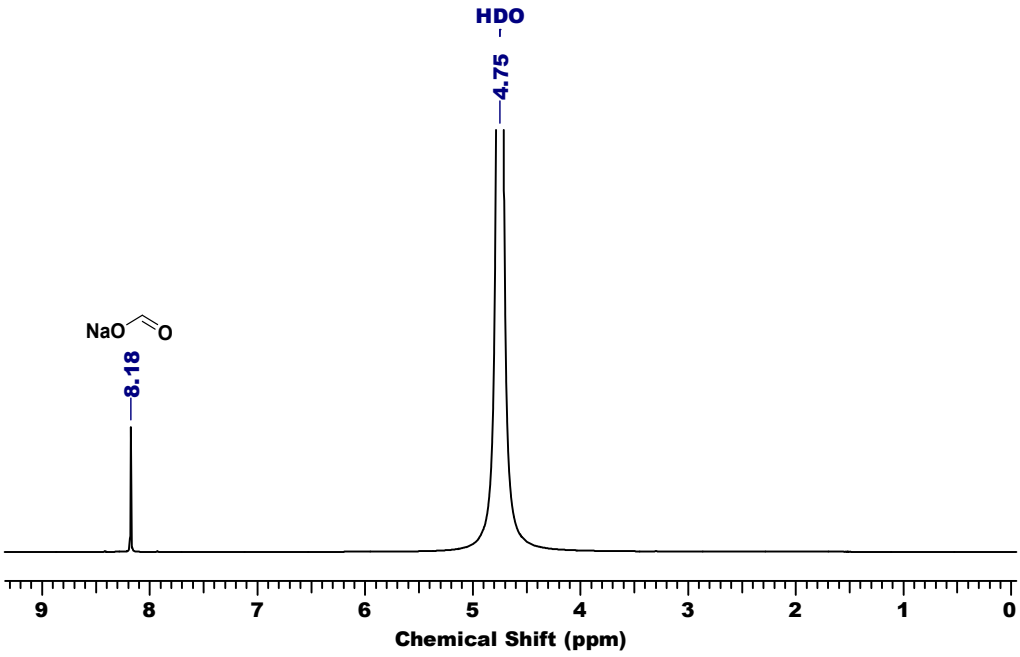

Fig. S30 ^{1}H NMR spectra of the crude reaction mixture of the catalytic reaction for hydrogen production from formic acid over Ru/La(OH)$_3$ catalyst. Reaction conditions: Ru/La(OH)$_3$ (100 mg, 9 wt% Ru), formic acid (13.68 mmol), NaOH (27.36 mmol), water (41.04 mmol), 130 °C, and 600 rpm.

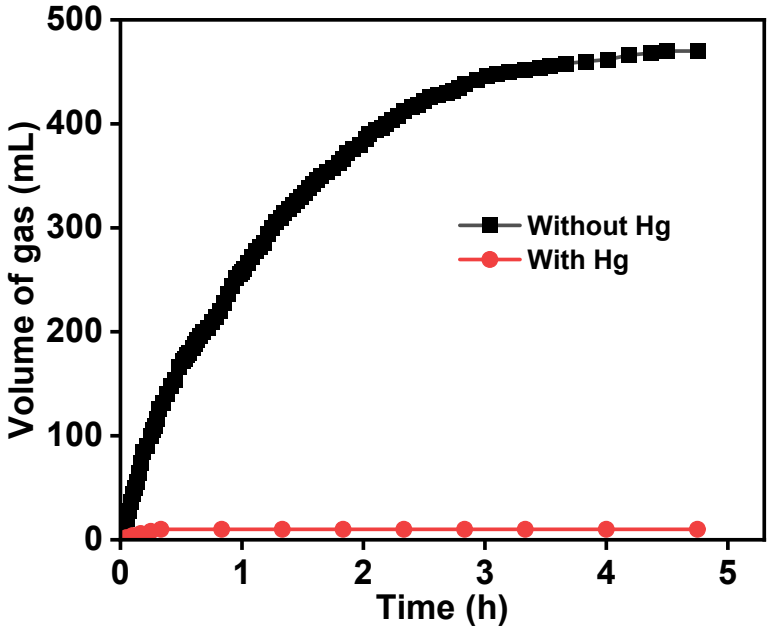

Fig. S31 Hg poisoning experiment to validate the heterogeneous of Ru/La(OH)$_3$ catalyst.

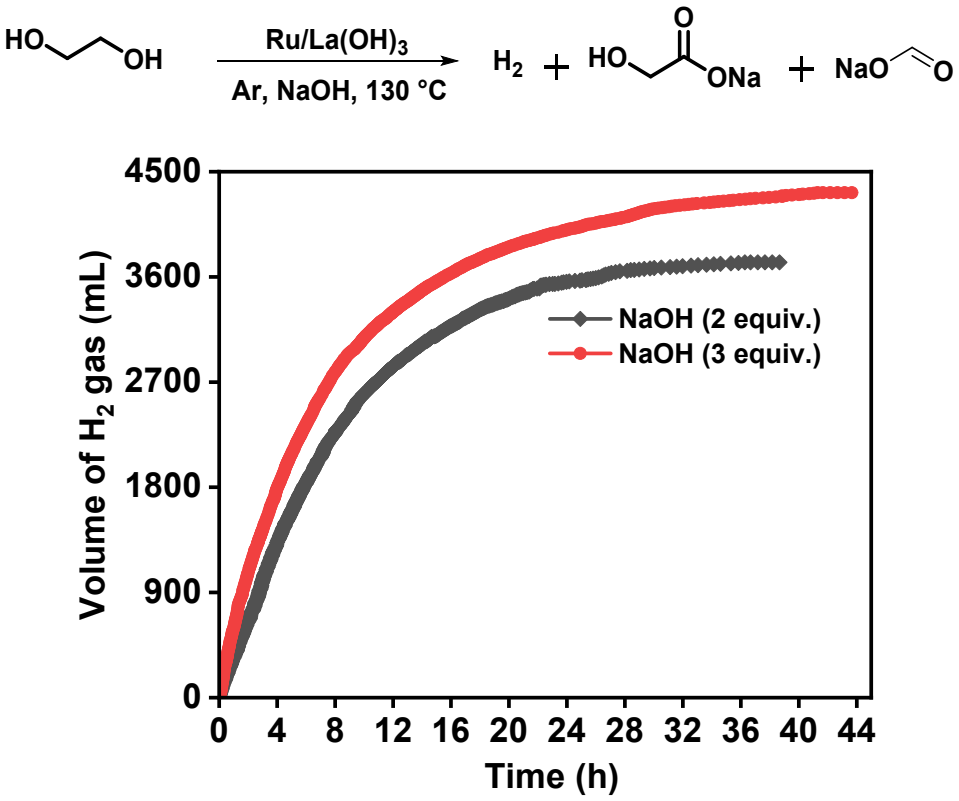

Fig. S32 Time course plot for the large-scale production of hydrogen gas from ethylene glycol over $Ru/La(OH)_3$ catalyst. Reaction conditions: $Ru/La(OH)_3$ (100 mg, 9 wt% Ru), ethylene glycol (68.4 mmol), NaOH, water (205.2 mmol), 130 °C, and 600 rpm.

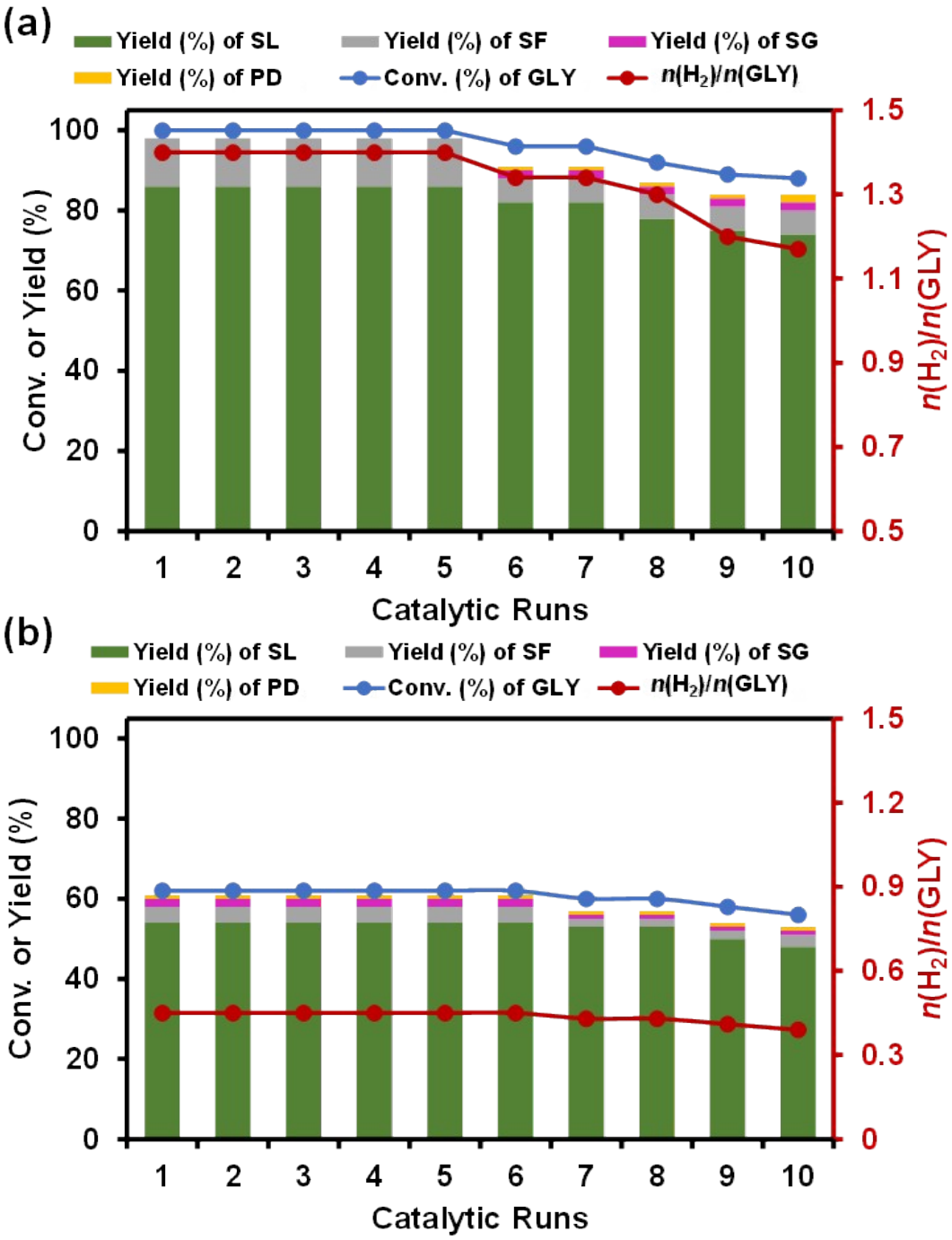

Fig. S33 Recyclability experiment for hydrogen production from glycerol over the Ru/La(OH)$_3$ catalyst at (a) initial complete GLY conversion and (b) intermediate GLY conversion (1.5 h). Reaction conditions: Ru/La(OH)$_3$ (100 mg, 9 wt% Ru), GLY (13.68 mmol), NaOH (27.36 mmol), water (41.04 mmol), 130 °C, and 600 rpm.

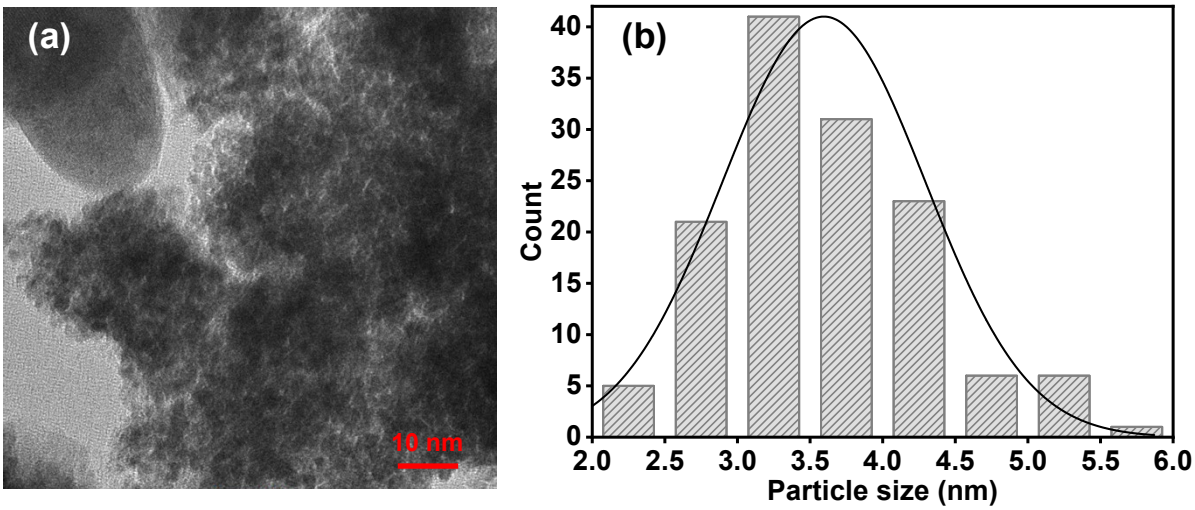

Fig. S34 (a) TEM image, and (b) corresponding particle size distribution graph of the recovered Ru/La(OH)$_3$ catalyst after ten cycles.

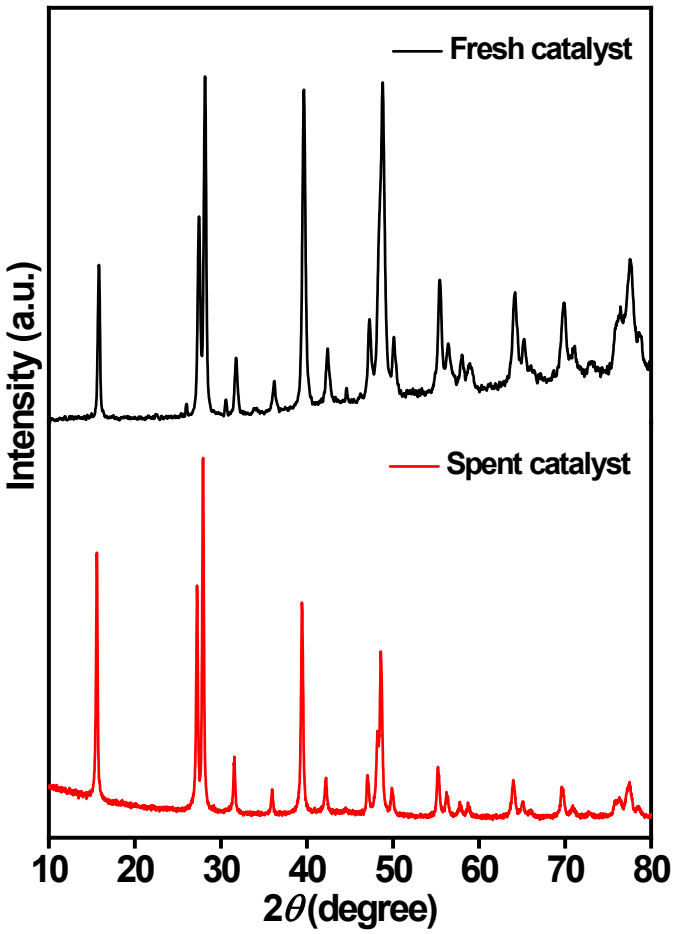

Fig. S35 P-XRD pattern of the spent Ru/La(OH)$_3$ catalyst.

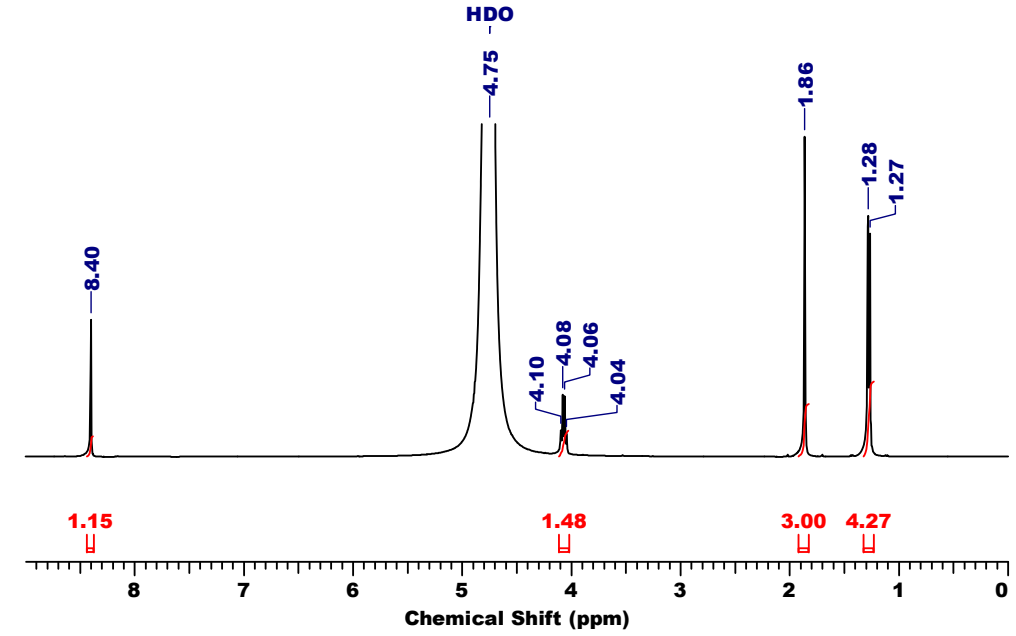

Fig. S36 ^{1}H NMR spectra of the crude reaction mixture of the catalytic reaction for hydrogen production from crude glycerol over the ruthenium catalyst. Reaction conditions: Ru/La(OH)$_3$ (100 mg, 9 wt% Ru), crude GLY (1.25 mL), NaOH (27.36 mmol), water (41.04 mmol), 130 °C, 7 h, and 600 rpm.

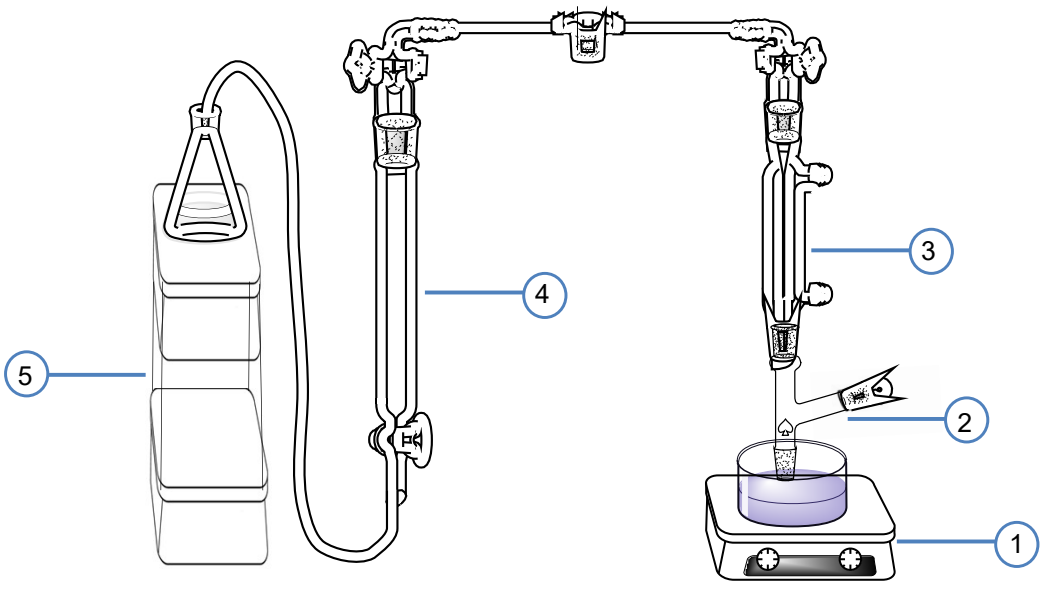

Fig. S37 Reaction setup for measuring the volume of gas generated during the catalytic dehydrogenation of glycerol over the ruthenium catalyst (1. Hot plate stirrer, 2. Two neck test tube, 3. Condenser, 4. Gas Burette, 5. Jack).

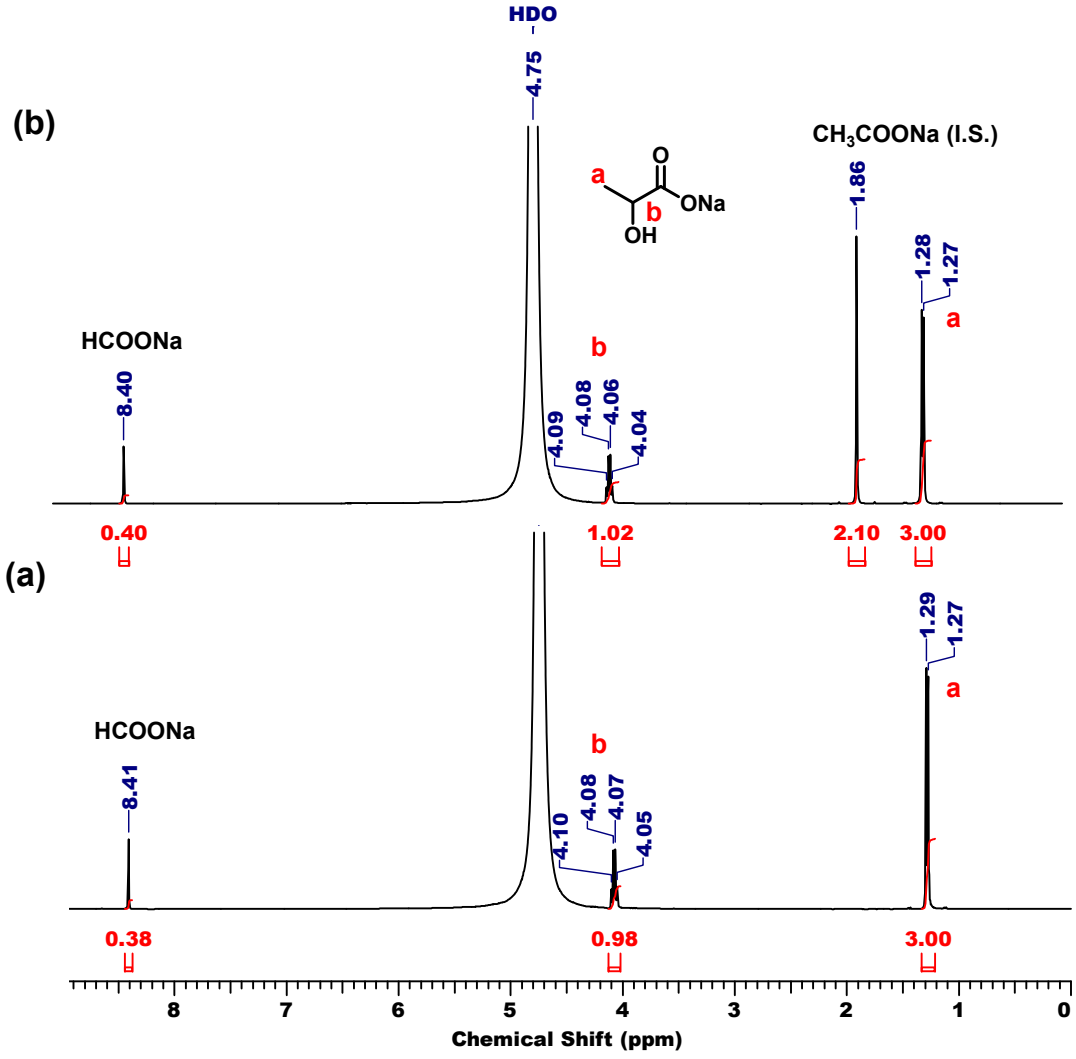

Fig. S38 ^{1}H NMR spectra of the crude reaction mixture (a) without sodium acetate as an internal standard, (b) with sodium acetate as an internal standard of the catalytic reaction in D_2O:H_2O (1:9) for hydrogen production from glycerol over $La(OH)_3$ catalyst. Reaction conditions: Ru/$La(OH)_3$ (100 mg, 9 wt% Ru), glycerol (13.68 mmol), NaOH (27.36 mmol), water (41.04 mmol), 130 °C, and 4.5 h.

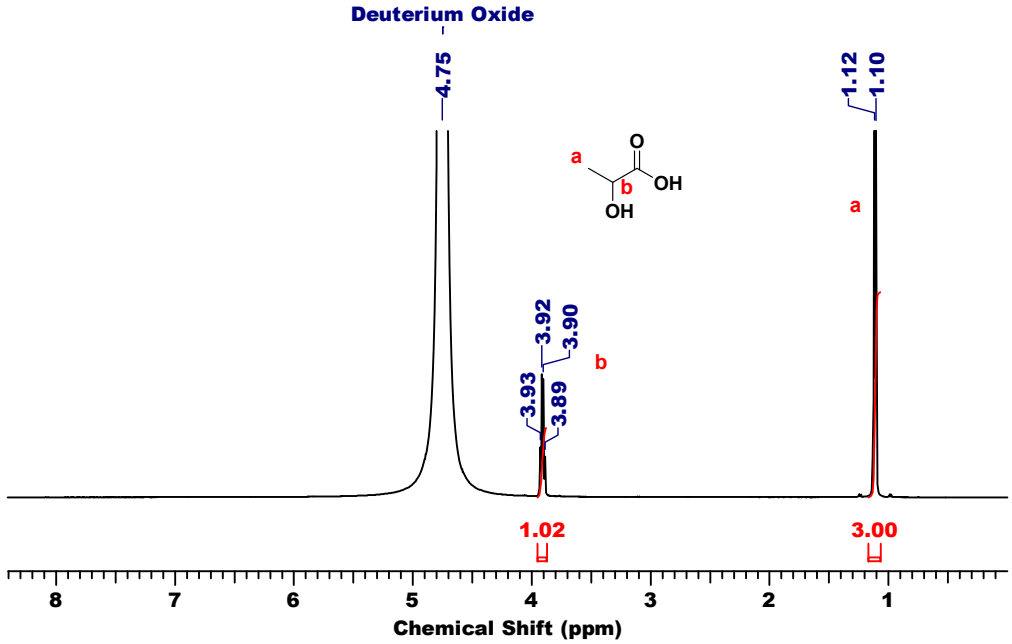

Fig. S39 ^{1}H NMR spectra of pure lactic acid in D_2O.

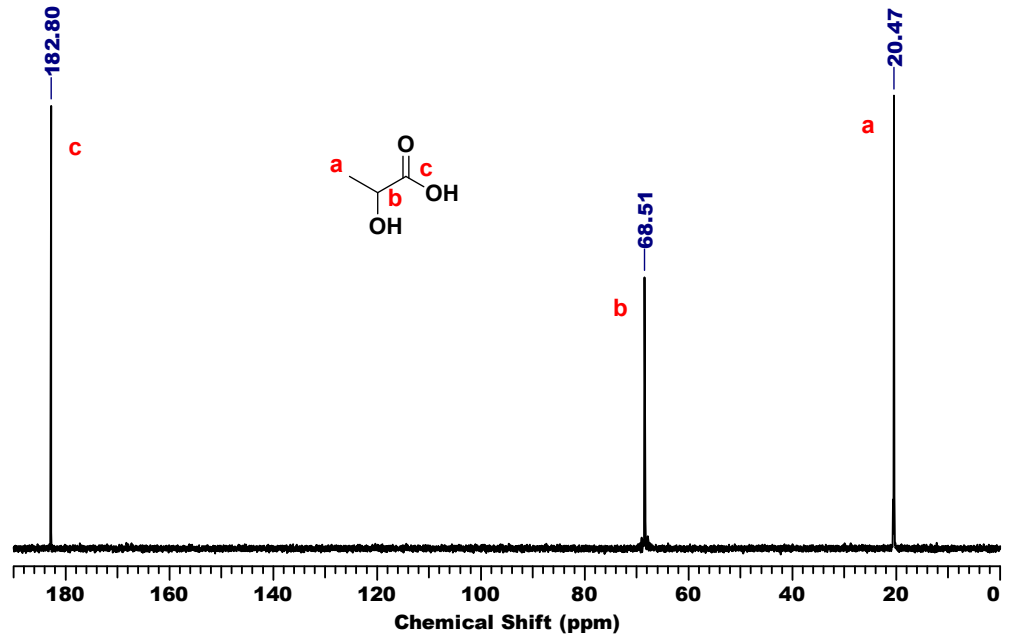

Fig. S40 ^{13}C NMR spectra of pure lactic acid in D_2O.

References.

S1 S. Patra, M. K. Awasthi, R. K. Rai, H. Deka, S. M. Mobin and S. K. Singh, *Eur. J. Inorg. Chem.* 2019, **2019**, 1046-1053.

S2 A. Kumar, M. K. Awasthi, B. Priya and S. K. Singh, *ChemCatChem*, 2022, **14**, e202101951.

S3 P. Gogoi, N. Kanna, P. Begum, R. C. Deka, C. V. V. Satyanarayana and T. Raja, *ACS Catal*., 2020, **10**, 2489-2507.

S4 G. Bergeret and P. Gallezot, Wiley-VCH Verlag, 2008, 738-765.

S5 P. Gogoi, A. S. Nagpure, P. Kandasamy, C.V. V. Satyanarayana and T. Raja, *Sustain. Energy Fuels*, 2020, **4**, 678-690.

S6 P. J. Dietrich, R. J. Lobo-Lapidus, T. Wu, A. Sumer, M. C. Akatay, B. R. Fingland, N. Guo, J. A. Dumesic, C. L. Marshall, E. Stach, J. Jellinek, W. N. Delgass, F. H. Ribeiro and J. T. Miller, *Top. Catal*., 2012, **55**, 53-69.

S7 D. L. King, L. Zhang, G. Xia, A. M. Karim, D. J. Heldebrant, X. Wang, T. Peterson and Y. Wang, *Appl. Catal. B: Environ*., 2010, **99**, 206-213.

S8 A. Iriondo, V. L. Barrio, J. F. Cambra, P. L. Arias, M. B. Güemez, R. M. Navarro, M. C. Sánchez-Sánchez and J. L. G. Fierro, *Top. Catal*., 2008, **49**, 46-58.

S9 D. A. Boga, R. Oord, A. M. Beale, Y. M. Chung, P. C. A. Bruijnincx and B. M. Weckhuysen, *ChemCatChem*, 2013, **5**, 529-537.

S10 D. R. Cortright, R. R. Davda and J. A. Dumesic, *Nature*, 2002, **418**, 964-967.

S11 C. Pendem, B. Sarakar, N. Siddiqui, L. N. S Konathala, C. Baskar and R. Bal, *ACS Sustain. Chem. Eng*., 2018, **6**, 2122-2131.

S12 M. M. Rahman, *Catal. Lett*., 2020, **150**, 2674-2687.

S13 Y. Guo, X. Lui and Y. Wang, *Ind. Eng. Chem. Res*., 2019, **58**, 2749-2758.

S14 G. Wen, Y. Xu, H. Ma, Z. Xu and Z. Tian, *Int. J. Hydrog. Energy*, 2008, **33**, 6657-6666.

S15 K. Polychronopoulou, N. D. Charisiou, G. I. Siakavelas, A. A. Alkhoori, V. Sebastian, S. J. Hinder, M. A. Baker and M. A. Goula, *Sustain. Energy Fuels*, 2019, **3**, 673-691.

S16 T. Hirai, N. Ikenaya, T. Miyake and T. Suzuki, *Energy Fuels*, 2005, **19**, 1761-1762.

S17 S. Adhikari, S. Fernando and A. Haryanto, *Catal. Today*, 2007, **129**, 355-364.

S18 R. Sundari and P. D. Vaidya, *Energy Fuels*, 2012, **26**, 4195-4204.

S19 K. Kousi, D. I. Kondarides, X. E. Verykios and C. Papadopoulou, *Appl. Catal. A: Gen.*, 2017, **542**, 201-211.

S20 Z. Tang, P. Liu, H. Cao, S. Bels, H. J. Heeres and P. P. Pescarmona, *ACS Catal*., 2019, **9**, 9953-9963.

S21 Z. Jiang, Z. Zhang, T. Wu, P. Zhang, J. Song, C. Xie and B. Han, *Chem. Asian J*., 2017, **12**, 1598-1604.

S22 G. Zhang, X. Jin, Y. Guan, B. Yin, X. Chen, Y. Liu, X. Feng, H. Shan and C. Yang, *Ind. Eng. Chem. Res*., 2019, **58**, 14548-14558.

S23 G. Bharath, K. Rambabu, A. Hai, H. Taher and F. Banat, *ACS Sustain. Chem. Eng*., 2020, **8**, 7278-7289.

S24 W. Oberhauser, C. Evangelisti, C. Tiozzo, F. Vizza and R. Psaro, *ACS Catal*., 2016, **6**, 1671-1674.

S25 J. Ftouni, N. Villandier, F. Auneau, M. Besson, L. Djakovitch and C. Pinel, *Catal. Today*, 2015, **257**, 267-273.

S26 S. M. A. H. Siddiki, A. S. Touchy, K. Kon, T. Toyao and K. I. Shimizu, *ChemCatChem*, 2017, **9**, 2816-2821.

S27 E. P. Maris, W. C. Ketchie, M. Murayama and R. J. Davis, *J. Catal*., 2007, **251**, 281-294.

S28 L. Shen, Z. Yu, D. Zhang, H. Yin, C. Wang and A. Wang, *J. Chem. Technol. Biotechnol*., 2019, **94**, 204-219.

S29 M. Checa, F. Auneau, J. H. Carrillo, A. Marinasa, J. M. Marinasa, C. Pinel and F. J. Urbano, *Catal. Today*, 2012, **196**, 91-100.

S30 X. Jin, L. Dang, J. Lohrman, B. Subramaniam, S. Ren and R. V. Chaudhari, *ACS Nano*, 2013, **7**, 1309-1316.

S31 D. Roy, B. Subramaniam and R. V. Chaudhari, *ACS Catal*., 2011, **1**, 548-551.

S32 R. Palacio, S. Torres, S. Royer, A. S. Mamede, D. López and D. Hernández, *Dalton Trans*., 2018, **47**, 4572-4582.

S33 H. Yin, H. Yin, A. Wang and L. Shen, *J. Ind. Eng. Chem. Res.*, 2018, **57**, 226-235.

S34 D. G. Lahr and B. H. Shanks, *Ind. Eng. Chem. Res.* 2003, **42**, 5467-5472.

S35 S. Mondal, H. Malviya and P. Biswas, *React. Chem. Eng.* 2019, **4**, 595-609.